Energy Storage Materials 83 (2025) 104714

Contents lists available at ScienceDirect

Energy Storage Materials

journal homepage: www.elsevier.com/locate/ensm

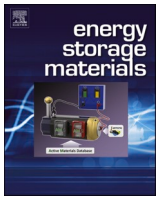

Tailoring aqueous electrolytes for low-temperature applications: from fundamentals to practical solutions

Liwen Pan [a], Nannan Jia [a], Jie Yang [b,*], Xinhua Liu [c,*], Rui Tan [d,*]

[a] School of Resources, Environment and Materials, Guangxi University, Nanning 530004, China
[b] Warwick Manufacturing Group, Energy Innovation Centre, University of Warwick, Coventry CV4 7AL, UK
[c] School of Transportation Science and Engineering, Beihang University, Beijing 100191, China
[d] Department of Chemical Engineering, Swansea University, Swansea SA1 8EN, UK

ARTICLE INFO

Keywords:
Low temperature
Aqueous battery
Electrolyte optimization strategy
Hydrogen bond network
Solvation structure

ABSTRACT

Aqueous batteries are promising candidates for grid-scale energy storage owing to their inherent safety and environmental sustainability; however, their low-temperature performance is hindered by electrolyte freezing and sluggish reaction kinetics. Electrolyte regulation has emerged as a key strategy to enable their operation under low-temperature conditions. This review first examines two fundamental mechanisms—hydrogen bond network and solvation structure evolution—which govern the thermodynamic and kinetic behavior of electrolytes at low temperatures. Building on these insights, we propose targeted electrolyte modifications and systematically summarize optimization strategies, including anion regulation, additives, co-solvents, eutectic electrolytes, salt selection, high-entropy system design, and novel solvation sheath engineering. Finally, we discuss current challenges and future research directions to advance low-temperature aqueous batteries through electrolyte innovation.

1. Introduction

The rapid increase in the consumption of fossil fuels has intensified global concerns over energy crisis and environmental pollution [1,2], driving urgent demand for safe, cost-effective, and scalable energy storage systems powered by renewables such as wind, solar, and tidal energy [3–5]. While lead-acid batteries and lithium-ion batteries (LIBs) currently dominate the market, their widespread adoption is hindered by the former's high toxicity and the latter's safety risks and high cost [6]. These limitations have prompted researchers to explore alternative batteries. Aqueous batteries—with their inherent safety, low cost, and eco-friendliness—have emerged as promising alternatives for grid-scale storage. These systems leverage diverse charge carriers (e.g., Li^+, Na^+, Zn^{2+}, Al^{3+}, H^+, NH_4^+) to achieve relatively competitive energy densities compared to LIBs, underscoring their potential as sustainable alternatives [7–9].

While aqueous batteries offer inherent safety—a critical requirement for large-scale energy storage—their limited temperature adaptability remains a fundamental barrier to widespread deployment. Currently constrained to an operating range of 10–40 °C [10,11], these systems are suitable for subtropical climates but fail to meet the needs of extreme environments. In high-latitude regions (e.g., Northern Europe, North America, East Asia) and polar research stations, where temperatures frequently fall below −20 °C, the demand for reliable low-temperature energy storage far surpasses that for high-temperature solutions. Sub-zero conditions induce electrolyte freezing and sluggish reaction kinetics, severely compromising battery stability and specific capacity. Consequently, enhancing the low-temperature performance of aqueous batteries is imperative to enable their practical application in diverse climates.

The deterioration of low-temperature performance in aqueous batteries stems from the synergistic interplay between hydrogen bond (HB) networks [12] and solvation behavior. At room temperature, water molecules form a short-range network of dynamic equilibrium through hydrogen bonds, with a high proportion of free water molecules available for rapid solvation. However, as temperature decreases, reduced molecular kinetic energy shifts this equilibrium, causing hydrogen bond formation to dominate over dissociation, thus gradually constructing a long-range ordered HB network structure[13]. This network effectively "anchors" a substantial number of water molecules into a rigid framework through hydrogen bonds[14], significantly reducing the population of free water. As a result, the remaining free water molecules are

* Corresponding authors.
E-mail addresses: jie.yang.5@warwick.ac.uk (J. Yang), liuxinhua19@buaa.edu.cn (X. Liu), rui.tan@swansea.ac.uk (R. Tan).

https://doi.org/10.1016/j.ensm.2025.104714
Received 11 September 2025; Received in revised form 22 October 2025; Accepted 22 October 2025
Available online 7 November 2025

compelled to coordinate with ions in a more ordered way. For example, water molecules surrounding Zn^{2+} become more tightly arranged, forming solvation sheaths with higher coordination numbers and enhanced bonding strength. These structures exhibit high de-solvation energy barriers that impede the movement of charged species while simultaneously reinforcing the local HB network through their anchoring effect on surrounding water molecules. This mutual reinforcement between solvation structure and HB network results in dual degradation mechanisms: increased electrolyte viscosity hindering ion transport and high de-solvation energy barriers slowing interfacial reactions at low temperatures. These effects are operationally evident through a marked reduction in battery capacity, increased internal resistance, and impaired charge–discharge performance. Addressing these challenges requires fundamental understanding and precise manipulation of both HB network and solvation structures in electrolytes, which is the key to improving low-temperature battery performance. The complex temperature-dependent thermodynamics and kinetics of these systems make stable cycling particularly challenging across different temperature ranges.

Significant advances in electrolyte engineering have been achieved in recent years, with multiple strategies demonstrating effectiveness in optimizing aqueous electrolytes[15–17]. Current approaches include composition optimization, additive incorporation, eutectic electrolyte formulation, co-solvent addition, salt-in-water electrolyte (WiSE) design, and solvation structure engineering. These modifications primarily function by disrupting the native hydrogen bond network of water molecules, thereby depressing the freezing point of electrolytes and enabling stable low-temperature battery operation. Simultaneously, the introduced chemical species interact electrostatically with charge carriers, facilitating solvation shell reconstruction[18,19]. This dual mechanism not only enhances low-temperature performance but also mitigates deleterious parasitic reactions that commonly plague aqueous battery systems. Besides the electrolyte optimization strategy [20], interface engineering[21] and electrode modification engineering[22], etc.[23–26], also contribute to improved low-temperature behavior. Fig. 1

Despite notable progress in developing low-temperature aqueous electrolytes through diverse empirical strategies, the existing reviews mainly emphasize macroscopic outcomes, leaving a critical gap in connecting these advances to their underlying microscopic principles. This review distinguishes itself by addressing that gap through focusing on two fundamental microstructural determinants: the thermodynamic and kinetic evolution of HBs, and the temperature-dependent behavior of ionic solvation sheaths, particularly their influence on de-solvation energy barriers. We systematically examine key optimization strategies such as high-concentration electrolytes, co-solvent systems, and additive engineering by regulating HB network dynamics and reconstructing solvation stability. To illustrate these principles, aqueous zinc-ion batteries are employed as a representative model, providing a mechanistic framework to guide the rational design of next-generation electrolytes for low-temperature applications.

2. Theoretical basis of low-temperature aqueous electrolytes

The electrolyte serves as the essential medium for ion transport between the anode and cathode, playing a pivotal role in the battery's electrochemical processes[27]. At low temperatures, however, the physical properties of aqueous electrolytes diverge markedly from their room-temperature behavior, primarily due to alterations in the hydrogen bond network of water molecules and the solvation structure of ions. To elucidate the fundamental mechanisms underlying electrolyte anti-freezing strategies, it is imperative to investigate the thermodynamic and kinetic properties of hydrogen bond networks under low-temperature conditions, as well as the interactions and stability of solvation shells. Such an in-depth study will provide critical insights for optimizing electrolyte performance in low temperature environments.

2.1. Thermodynamics and kinetics of hydrogen bond networks at low temperatures

2.1.1. Coordination structure of low-temperature hydrogen bond networks

Water molecules typically form HBs with up to four neighboring molecules, resulting in a stable tetrahedral coordination structure (Fig. 2**a**), which dynamically propagates through thermal motion[29]. The heterogeneous structure of liquid water at room temperature can be revealed by using small-angle X-ray scattering (SAXS), X-ray emission spectroscopy (XES), and X-ray Raman scattering (XRS)[30]. This structural heterogeneity is often interpreted as an extension of the liquid-liquid critical point (LLCP) in the "single-phase region," known as the Widom line effect. On the low-temperature side (near the LLCP), water predominantly exhibits a low-density tetrahedral structure, whereas the high-temperature side (far from the LLCP) is dominated by a high-density distorted structure. Despite these differences, liquid water maintains macroscopic homogeneity through dynamic equilibrium, while dynamic heterogeneity persists across varying temperatures and pressures.

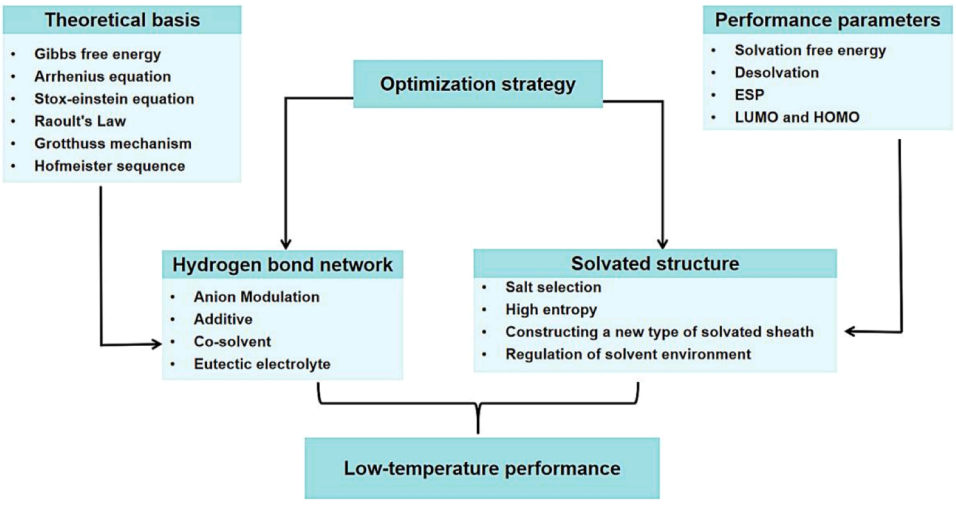

Fig 1. Relationship between theoretical basis/performance parameters and different optimization strategies, hydrogen bond network regulation and solvation structure jointly construct low-temperature performance.

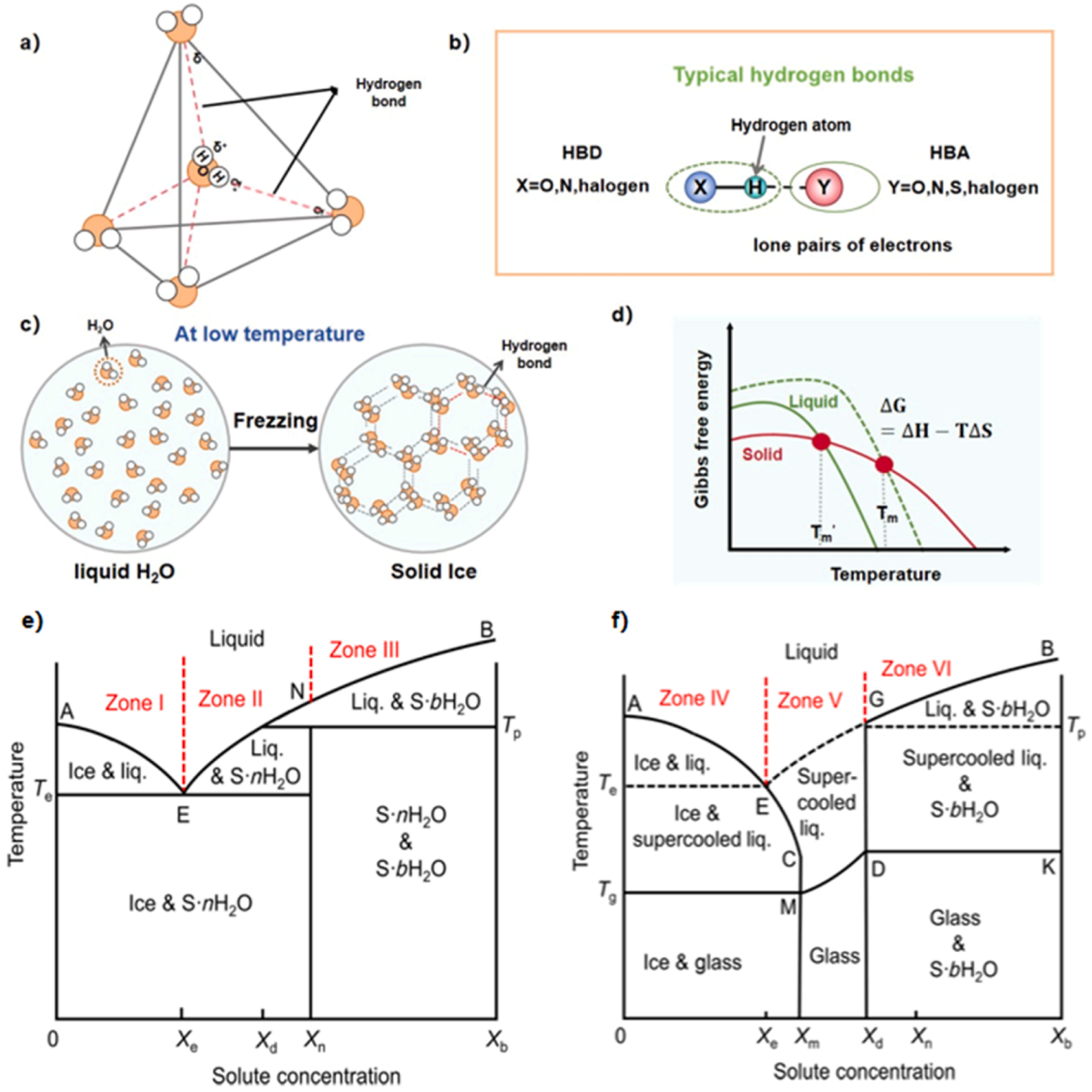

Fig. 2. Thermodynamics and kinetics of low-temperature hydrogen bond (HB) network. a) Coordination structure of water molecules. b) Typical hydrogen bond. c) Disordered water molecules transform into ice with an ordered hydrogen bond network as the temperature decreases. d) Relationship between Gibbs free energy, enthalpy and temperature. (e) Equilibrium binary (H_2O-solute) phase diagram. AE is the water-freezing curve, and BE is the solute-precipitation curve. T_e is the eutectic temperature of solutions at concentrations between 0 and X_n. T_p is the peritectic temperature of solutions at concentrations between X_d and X_b [28]. (f) Non-equilibrium binary (H_2O-solute) phase diagram. T_g is the glass transition temperature of solutions at concentrations between 0 and X_m. MDK is the T_g curve of solutions at concentrations between X_m and X_b [28].

HBs are characterized by their distinct saturation and directionality properties, typically represented as X-H···Y, where X-H serves as the hydrogen bond donor (HBD)[31]. The small size of the hydrogen atom restricts HB formation to a single acceptor atom (Y), while electrostatic repulsion between electronegative atoms further enforces this saturation [32]. Directionality arises from the alignment of electric dipole moments, with maximum HB strength achieved when X-H and Y adopt a linear configuration[33]. This optimal geometry (Fig. 2**b**) minimizes repulsion while allowing the lone electron pairs of Y (commonly N, O, S, or halogens) to interact efficiently with the hydrogen atom, analogous to covalent orbital overlap [34]. The bond energy of HBs is governed by two key factors: (1) the electronegativity of X and Y—higher electronegativity enhances bonding strength—and (2) the atomic radius of Y, with smaller radii promoting stronger interactions due to reduced donor-acceptor distances[35]. Consequently, HB strength increases with greater electronegativity and smaller atomic sizes of the participating atoms[36]. Water molecules connected by hydrogen bonds (HBs) organize into a dynamic, tetrahedral ice-like network, where continuous thermal motion drives the simultaneous breaking and reformation of intermolecular HBs[37]. Above 4 °C, the kinetic energy of water molecules dominates over HB interactions, maintaining a pervasive HB network where less than 1 % of molecules remain unbound[38]. This fluctuating network serves as the foundation for subsequent ice nucleation. As temperature decreases, the reduced kinetic energy progressively favors HB stabilization, leading to increased structural ordering [39]. When the temperature is below 4 °C, strengthened HB interactions constrain molecular motion, manifesting as elevated viscosity and diminished fluidity[40]. This process culminates in complete solidification when the temperature reaches the freezing point, transforming liquid water into crystalline ice (Fig. 2**d**).

Therefore, the fundamental strategy for preventing ice crystallization lies in disrupting the HB network of water. This can be achieved by suppressing the development of ordered HB structures during cooling process, which effectively depresses the freezing point of aqueous electrolytes. Such an approach significantly improves the low-temperature electrochemical performance of energy storage systems

by maintaining ionic mobility and electrolyte stability at low temperatures.

2.1.2. Kinetics of hydrogen bond networks at low temperatures

The dynamic evolution of HB networks at low temperatures constitutes a fundamental mechanism underlying the performance deterioration of aqueous electrolytes. At the molecular level, the kinetics of HB breakage and reformation critically determine electrolyte behavior, as these dynamics govern both the structural organization and mobility of water molecules. In a computer model of liquid water,an instantaneous configuration, r(t), denotes the positions of all the atoms in the system at time t. A configurational criterion for whether a particular pair of water molecules is bonded allows one to define a hydrogrn bond population operator, h[r(t)] $= h$(t). This operator has a value 1 when the particular tagged pair,say molecules 1 and 2, are bonded, and zero otherwise. The average number of hydrogen bonds in an equilibrium fluid of N water molecules is $\frac{1}{2}N(N-1)\langle h\rangle$, where $\langle h\rangle$ denotes the average of h[r(t)][41], The angular brackets indicate that the averaging is performed over different time origins. The H-bond structure in liquid water markedly fluctuates and is often studied theoretically through H-bond population correlation variables[42]. Hydrogen bonds are typically defined using geometric criteria [43], while their temporal characteristics are quantified through two key correlation functions: the continuous hydrogen bond correlation function S(t) and the intermittent hydrogen bond correlation function C(t) [44,45]. These functions provide essential insights into the timescales of HB reorganization under low-temperature conditions.

$$S(t) = \frac{\langle h(0)H(t)\rangle}{\langle h\rangle}$$

$$C(t) = \frac{\langle h(0)h(t)\rangle}{\langle h\rangle}$$

The definition presented above relies on two key variables that characterize hydrogen bond distribution: h(t) and H(t). The variable h(t) is assigned a value of 1 when a specific site is engaged in a hydrogen bond at time t, and 0 otherwise. In contrast, H(t) is defined as 1 only if the designated site pair has continuously maintained a hydrogen bond from the initial time $t = 0$ up to time t; if the bond is broken at any point during this interval, H(t) becomes 0. h(0) indicates that the hydrogen bond remains intact at time $t = 0$[46]. Based on these definitions, the function S(t) quantifies the probability that a hydrogen bond formed at time zero remains uninterrupted until time t, thereby offering a rigorous metric for assessing hydrogen bond lifetimes. However, the C(t) describes the probability that a hydrogen bond is intact at time t, given it was intact at time zero, independent of possible breaking in the interim time. This allows for transient bond breakage and reformation, including the possibility of barrier re-crossing between bonded and non-bonded states and long-term diffusive behavior. Consequently, the relaxation behavior of C(t) provides insight into the structural relaxation of hydrogen bonds. To estimate the relaxation time of hydrogen bonds in water, this microscopic kinetic framework can be linked to a phenomenological description of the reaction process. For example, HB breaking/reforming:

$$A \rightleftarrows B$$

Let K and K' denote the forward and reverse rate constants, respectively. When the system undergoes multiple transitions between the reactant state A and the product state B, it eventually reaches a state of dynamic equilibrium. Assuming that each hydrogen bond behaves independently and that subsequent re-crossings between states are statistically irrelevant [47], the reaction time constant $\tau=(K + K')^{-1}$ serves as a characteristic measure of the system's transition dynamics from state A to state B. According to the detailed balance situation [48]:

$$\frac{1-\langle h\rangle}{\langle h\rangle} = \frac{K}{K'}$$

Therefore, the characteristic relaxation time τ is related to the rate constant K of HB breaking[49]:

$$\tau = \frac{1-\langle h\rangle}{K}$$

The relationship between the rate constant K of HB breaking and the equivalent average HB lifetime is described as below:

$$\tau_{HB} = 1/K$$

The HB breaking rate constant K follows the Arrhenius equation[50,51]:

$$K = \sigma_0 exp\left(-\frac{E_{a1}}{K_b T}\right)$$

where A is the pre-exponential factor, E_{a1} is the apparent activation energy, T is the absolute temperature, and K_b refers to the reaction rate. The average lifetime of HB shows an approximate Arrhenius-type dependence on temperature[52]. This temperature-dependent increase in HB lifetime underlies the microdynamic mechanism responsible for the performance degradation of aqueous batteries at low temperatures. This trend can be disrupted through the introduction of HB disruptants that interfere with the stability of the bonding network.

Another critical process affected by low temperatures in electrochemical systems is charge transfer, which becomes the dominant limiting factor below −20 °C. As temperature decreases, electrolyte viscosity increases significantly, leading to reduced ionic conductivity. This deterioration in transport properties severely constrains the electrochemical performance of water-based batteries, particularly under high-rate charging conditions[28]. According to the Stoke-Einstein equation[53,54], the ionic conductivity σ of an electrolyte can be mathematically expressed by the following formula[55]:

$$\sigma = \sum_i (n_i \mu_i Z_i e)$$

$$\mu_i = \frac{1}{6\pi\eta r_i}$$

where Z_i, e, n_i, μ_i, η_i and r_i represent the valence, charge of the electrons, free ion numbers, ionic mobility, viscosity, and solvation radius of the ion i, respectively. Ionic conductivity is primarily governed by the concentration of free ions and their mobility. As the temperature of the electrolyte decreases, intensified HB restricts the movement of water molecules, leading to increased viscosity and reduced fluidity [40]. According to the above formula, elevated viscosity slows ion migration and diminishes ionic conductivity, further exacerbating the already sluggish electrochemical kinetics under low-temperature conditions.

2.1.3. Thermodynamics of hydrogen bond networks at low temperatures

The liquidus temperature of an electrolyte is fundamentally determined by the Gibbs free energy difference between its solid and liquid phases[56]. This thermodynamic framework governs all phase transition processes in electrolyte systems, including water-ice transformation and solute precipitation-dissolution equilibria. The relationship can be expressed through the following thermodynamic equation [57–59]:

$$\Delta G = \Delta H - T\Delta S$$

where ΔG, ΔH, T and ΔS represent the Gibbs free energy change, enthalpy change, temperature change and entropy change of the actual electrolyte system, respectively. As shown in Fig. 2**e,f**[28], the water freezing curve AE and the solute precipitation curve BE merge at the eutectic point, forming a V-shaped curve. To understand the AE and BE curves, it is first necessary to determine the phase transition temperature

T_m on this V-shaped curve. At the solid-liquid transition temperature (T_m), the system reaches phase equilibrium, resulting in $\Delta G = 0$. Consequently, T_m is determined by the ratio of enthalpy change to entropy change ($\Delta H/\Delta S$), as expressed in Equation[28]:

$$T_m = \frac{\Delta H}{\Delta S} = \frac{H_{soln} - H_{ice} - H_{M\cdot nH_2O}}{S_{soln} - S_{ice} - S_{M\cdot nH_2O}}$$

Among them, T_m is the phase transition temperature; H_{soln}, H_{ice} and $H_{M\cdot nH_2O}$ represent the enthalpy of the solution, ice and hydrated salt $M\cdot nH_2O$, respectively; S_{soln}, S_{ice} and $S_{M\cdot nH_2O}$ are the entropies of solution, ice and $M\cdot nH_2O$, respectively. During the phase transition from solid (e.g., ice and hydrated salt ($M\cdot nH_2O$)) to aqueous solution below T_m, the strongly hydrogen-bonded ice and electrostatically bound $M\cdot nH_2O$ crystals dissociate into a disordered solution of anions, cations, and water molecules. This process reduces the system's enthalpy (ΔH) due to the replacement of strong solid-phase interactions with weaker solute-solvent interactions, while the entropy (ΔS) increases as ordered crystals transform into a disordered liquid phase. Thermodynamically, a lower ΔH and higher ΔS directly reduce the solid-liquid transition temperature (T_m), as $T_m = \Delta H/\Delta S$. Since the enthalpies and entropies of pure ice and solutes are typically fixed, lowering T_m requires reducing the aqueous electrolyte's enthalpy (e.g., via strong ion–solvent or polymer–water interactions) and increasing its entropy (e.g., by disrupting the hydrogen-bond network). As illustrated in Fig. 2**c**, these synergistic effects—weakened intermolecular forces and enhanced disorder—collectively depress the freezing point of the electrolyte.

The anti-freezing performance of aqueous electrolytes exhibits a strong dependence on solute concentration, with this relationship predominantly governed by Raoult's law[60]:

$$\Delta T_f = T_{Water} - T_{Electrolyte} = K_f \times m$$

Where ΔT_f represents the change in freezing point, T_{Water} is the freezing point of pure water (0 °C, 1atm); $T_{Electrolyte}$ is the freezing point of the electrolyte; K_f is the constant for the decrease in freezing point of the solvent (1.86 °C kg mol^{-1} for water); and m is the molar concentration of the ion (m: mol kg^{-1}, molar concentration)[61]. In extremely dilute electrolytes, ion concentration exerts minimal influence on freezing point depression due to the overwhelming predominance of water molecules; the sparse hydrated ions cannot effectively disrupt the hydrogen bond network, leading to rapid ice formation below 0 °C[62]. While Raoult's law provides a framework for freezing point prediction, its applicability fails for concentrated electrolytes where the amount of hydrated water gradually increases with the increase of solute content [63]. When the solute concentration surpasses a critical threshold, the availability of water molecules becomes insufficient to fully coordinate with all ions. At extremely high concentrations, the strong pair between metal ions and oxygen strongly rearranges the coordination structure of water. Water molecules are almost entirely used for hydrated ions, and the original hydrogen bond network is almost completely destroyed [40].

However, some aqueous solution batteries can operate at temperatures below T_f[28]. A typical H_2O- solute equilibrium phase diagram shows that, compared with T_f, T_e is the thermodynamic temperature-limiting factor that determines battery operation. Fig. 2**e** exhibits a typical temperature–component binary (H_2O-solute) equilibrium phase diagram[64]. The equilibrium phase diagram can be divided into three zones (zones I, II and III). Both the aqueous solutions in Zone I and Zone II undergo the eutectic crystallization process below the eutectic temperature T_e. The solution in zone III underwent an peritectic crystallization process below the peritectic temperature T_p. Fig. 2**f** displays a typical temperature-component binary (H_2O-solute) non-equilibrium phase diagram. It keeps the basic framework of the equilibrium phase diagram except for additional supercooling and glass state zones. Solutions of different concentrations exhibit different phase transition behaviors along with temperature decreasing. Among the concentrations between 0 and X_e, the solutions would experience gradual ice precipitation process below curve AE and keep the supercooling liquid state below T_e until becoming the glass state below kinetic glass-transition temperature(T_g). In the X_e-X_m concentrations zone, thesupercooling liquid state below GE, ice precipitation process under curve EC, and it becomes glassy below T_g. The concentration range of X_m-X_d, the supercooling liquid state below GE, and the glassy state below MD. For the X_d-X_b concentration region, the aqueous solution undergoes a gradual precipitation process of hydrated solute below the curve BG, and then the remaining solution remains in a supercooling state below T_p until it turns into a glassy state under the DK curve. Based on the above description of the phase diagram, it can be found that electrolytes of different concentrations usually have different T_f (T_f is the temperature at which the electrolyte begins to freeze and is in a partially frozen state), but they have the same T_e (T_e is the temperature at which the electrolyte is completely frozen), and $T_f \geq T_e$. So T_f does not represent the true thermodynamic limit for anti-freezing behavior[65]. Instead, the T_e defines the lowest equilibrium temperature at which a liquid phase can exist. T_g is a kinetic decisive temperature-limiting factor for low-temperature batteries and is only applicable for H_2O-solute systems with strong super-cooling ability (SCA). T_g governs the kinetic stability of deeply supercooled electrolytes.

Thermodynamic analysis suggests that an effective anti-freezing strategy should involve reducing the enthalpy change (ΔH) by strengthening interactions among electrolyte components, while simultaneously increasing the entropy (ΔS) through the introduction of additional constituents. Additionally, a moderate increase in solute concentration further contributes to improved low-temperature performance. In addition to focusing on reducing T_f to inhibit ice formation, extreme low-temperature performance should also pay attention to strategies for low T_e and strong subcooling capacity.

2.1.4. Relationship between hydrogen bond networks and electrochemical performance

The electrochemical performance of a system is closely linked to the thermodynamics and kinetics of its hydrogen bond (HB) network. As secondary bonds, HBs exhibit strong electrostatic interactions that critically influence the transport mechanisms of protons, OH^-, NH_4^+ ions, and other hydrogen bond donors (HBDs), as well as Grotthuss-based diffusion pathways. Water molecules form a dynamic yet structurally ordered HB network, which can significantly hinder ion mobility. This impediment arises from the requirement that ions need to disrupt the surrounding HBs to migrate through the aqueous medium, thereby introducing an energetic barrier to diffusion. The influence of ions on water structure generally follows the Hofmeister series (Fig 3**a**)[66], with hydration capacity strongly dependent on surface charge density [57]. Small, highly charged ions act as "structure makers," stabilizing the HB network through strong hydration effects, whereas large, weakly charged monovalent ions ("structural disruptors") destabilize the ordered arrangement of water molecules, enhancing non-polar solute solubility and weakening aggregate stability. Notably, high-charge-density anions generate intense local electric fields, inducing tighter packing of solvation-shell water molecules [67,68]. At low temperatures, structural disruptors further destabilize the HB network, significantly lowering the system's freezing point [69].

The Grotthuss mechanism describes the efficient conduction of protons (H^+) through a hydrogen bond (HB) network via coordinated proton transfer, analogous to the motion of Newton's cradle (Fig 3**b**) [70]. In this process, a proton jumps between adjacent water molecules within the HB network, displacing another hydrogen atom and propagating this transfer in a chain-like manner (Fig 3**c**) [71]. Crucially, proton transport occurs through a relay mechanism along HB chains rather than physical diffusion. This mechanism relies on the dynamic disorder of the HB network: sufficiently short HB lifetimes enable frequent proton jumps, while network connectivity ensures

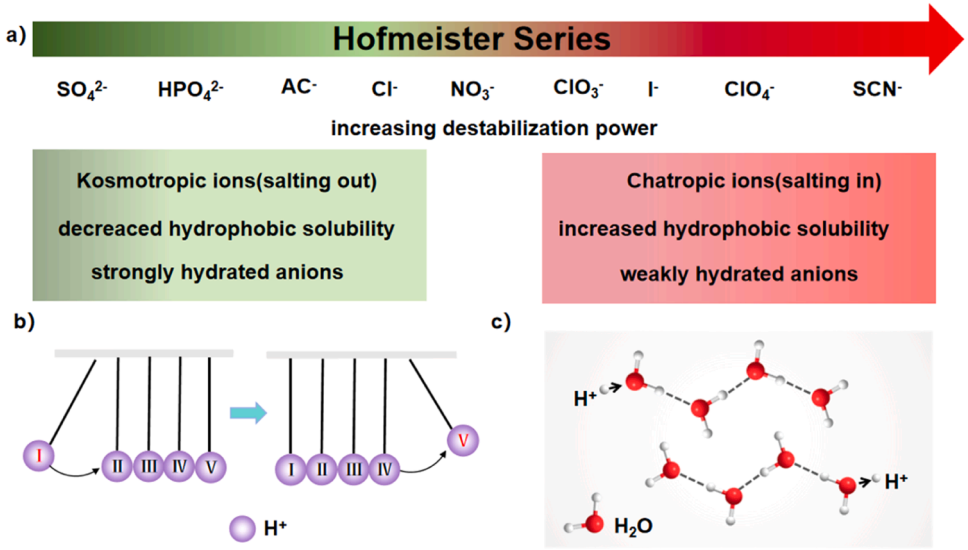

Fig 3. Relationship between hydrogen bond networks and electrochemical performance. a) Hofmeister sequence. b) Newton's cradle model. c) The diffusion pathways of Grotthuss.

uninterrupted pathways. The Grotthuss mechanism plays a pivotal role in facilitating redox reactions and ion insertion, particularly beneficial in aqueous metal-ion batteries by enabling additional proton storage. As a result, HB chemistry improves both rate capability (power density) and specific capacity (energy density), especially under high current densities. Furthermore, HB-mediated attraction and confinement of H_2O molecules reduce the energy barrier for de-solvation. Modifying the HB environment of water molecules also suppresses their reactivity, thereby inhibiting H_2O decomposition and mitigating side reactions.

The current understanding of low-temperature HB network encompasses a multi-scale theoretical framework. Structurally, the heterogeneity of liquid water originates from the Widom line effect near the liquid-liquid critical point (LLCP), where hydrogen bond saturation and directionality maintain tetrahedral coordination. Kinetically, the Arrhenius temperature dependence of HB lifetimes governs performance degradation at low temperatures, as increased viscosity and reduced ion mobility impair conductivity—though existing models inadequately reflect network synergy effects. Thermodynamically, high-concentration electrolytes deviate from Raoult's law due to competitive hydration, necessitating coordinated suppression of ice nucleation via reduced enthalpy change (ΔH) and enhanced entropy change (ΔS). Electrochemically, the Hofmeister series guides ion selection, while the Grotthuss proton conduction mechanism depends on dynamic disorder and connectivity within the HB network. Despite recent advances, several critical challenges remain unresolved. First, the validity of the liquid–liquid critical point (LLCP) model under extreme conditions has yet to be conclusively verified. Second, high-concentration aqueous systems currently lack a unified and comprehensive thermodynamic framework. Third, while HB disruptors offer a promising strategy for modulating water structure, their use may inadvertently trigger undesirable side reactions, compromising system stability. To address these issues, future research should adopt an integrative approach that combines molecular simulations, in situ spectroscopic techniques, and machine learning methodologies. Such a strategy would enable the establishment of a quantitative "structure–dynamics–performance" relationship, thereby guiding the rational design of next-generation aqueous batteries with enhanced low-temperature performance.

2.2. Formation and evolution of solvated structures

The thermodynamic parameters governing zinc ion solvation and electrolyte stability—such as electrostatic potential (ESP), dielectric constant, and molecular orbital energy—are systematically examined. Within the framework of aqueous electrolyte formulation, the intrinsic properties of key components, including metal salts, solvents, and additives, as well as their mutual interactions (e.g., cation–anion coordination, cation–solvent interactions, and solvent–solvent dynamics), are analyzed in detail. Subsequently, the solvation structure of the cation is characterized through geometric descriptors and thermodynamic metrics, providing a comprehensive understanding of its coordination behavior and stability.

2.2.1. Formation and main components of the solvated shell layer

The preparation of electrolytes involves dissolving metal salts in solvents to form homogeneous solutions, which are subsequently processed for battery integration[72]. In these systems, cations, anions, and solvent molecules interact to create a microstructure characterized by long-range disorder but short-range order. During dissolution, cation-solvent interactions disrupt the original ionic bonds between cations and anions. Due to the strong interaction between cations and other components, ion clusters will spontaneously form around the cation centers and migrate as ion clusters in the electrolyte rather than as isolated ions. Critically, the composition and structure of the solvation shell—dictated by these interactions—directly influence ion transport and interfacial processes[73]. Consequently, tailoring cation solvation behavior presents a viable strategy for enhancing battery electrochemical performance[74].

For example, the solvation state of Zn^{2+} ions is governed by multiple competing factors in zinc-ion batteries (ZIBs)[75]. In typical dilute aqueous electrolytes such as 2 M $ZnSO_4$, water molecules readily coordinate with Zn^{2+} ions due to their lone electron pairs[76]. Given the low Zn^{2+} to H_2O molar ratio (~1:56), zinc ions are extensively hydrated[77]. Density functional theory (DFT) calculations confirm that at room temperature, the $[Zn(H_2O)_6]^{2+}$ complex—comprising six water molecules in the primary solvation sheath—represents the most energetically stable configuration, highlighting the fully hydrated nature of zinc ion solvation[78]. The strong coordination between zinc ions and water molecules within the solvation sheath renders the bound H_2O more susceptible to dissociation into H^+ and OH^- compared to free water. This elevated reactivity of water-rich solvation structures is a key contributor to the low energy density and poor stability of aqueous zinc metal batteries (AZMBs)[79]. Consequently, designing dehydrated solvation environments around zinc ions presents a promising strategy to overcome these limitations and enhance the electrochemical performance of

AZMBs[80].

In electrolyte systems, the solvation shell (or solvation layer) represents a fundamental structural framework where cations interact competitively with both solvent molecules and anions to form distinct ionic solvation structures[81]. When cation-dipole (cation-solvent) interactions dominate over cation-anion interactions, solvent molecules preferentially occupy the solvation shell, excluding anions and forming solvent-separated ion pairs (SSIP)[82](Fig. 4). In contrast, stronger cation–anion interactions promote the incorporation of anions into the solvation shell, resulting in contact ion pairs (CIP) or aggregates (AGG). Aggregates may involve one anion coordinating with two cations (AGG-I) or multiple cations (AGG-II), as illustrated in Fig. 4 [83]. SSIP structures, characterized by solvation sheaths composed exclusively of solvent molecules, exhibit higher de-solvation energy barriers and diminished low-temperature performance[84]. In contrast, CIP and AGG, which incorporate anions into the solvation shell, reduce de-solvation resistance and significantly enhance electrolyte performance under low-temperature conditions[85]. This structure-property relationship underscores the importance of precisely controlling cation solvation environments, particularly through promoting anion participation in CIP or AGG formation, as a critical strategy for optimizing electrolyte performance with respect to both interfacial stability and low-temperature operation.

2.2.2. *De-solvation energy barriers at low temperature*

The solvation/de-solvation process can be divided into three independent steps as shown in Fig. 4: (I) cation dissolution and solvation, which governs electrolyte conductivity[79]; (II) cation migration through the solvent, a critical determinant of ionic conductivity; and (III) interfacial cation de-solvation, which dictates ion intercalation kinetics. Notably, all three processes are fundamentally driven by dynamic cation–solvent–anion interactions[86,87]. The above steps can be carried out simultaneously or in sequence, and each step has varying degrees of influence on the transport kinetics of cations at low temperatures. In Step I, the lattice energy of the salt is governed by cation–anion interactions, while cation–solvent interactions determine the solvation energy[88]. In Step II, ion migration is modulated by both cation–anion coordination and solvent–solvent interactions. Strong coordination between cations and anions can hinder the transport of solvated cations[89]. Similarly, strong interactions between solvent molecules, such as hydrogen bonds, can lead to increased viscosity, thereby inhibiting the mobility of ions. Both steps primarily affect electrolyte conductivity, thereby limiting the battery's rate performance. In contrast, Step III is a more complex process, which involves the de-solvation process, the decomposition of solvents and anions on the surface, crossing energy barriers, and migration through the solid-electrolyte interphase (SEI) layer[90].

SEI is defined as the solid-electrolyte interface first proposed by Peled in 1979[91]. Generally, SEI is composed of insoluble products formed through spontaneous reactions between metal anodes and electrolytes. This thermodynamically driven process initiates immediately upon metal-electrolyte contact, forming a surface layer whose thickness is governed by electron tunneling limitations. Contrary to being static, the SEI undergoes dynamic evolution during cycling, with continuous electrolyte decomposition contributing to its replenishment [92]. While SEI permits limited electron tunneling under certain conditions [93], its primary function lies in serving as a selective barrier that: (1) suppresses further electrolyte decomposition and (2) prevents solvent co-intercalation, thereby enhancing electrode-electrolyte compatibility. Notably, the electrolyte solvation structure also influences SEI properties, which represents a complementary perspective to conventional SEI theory[94].

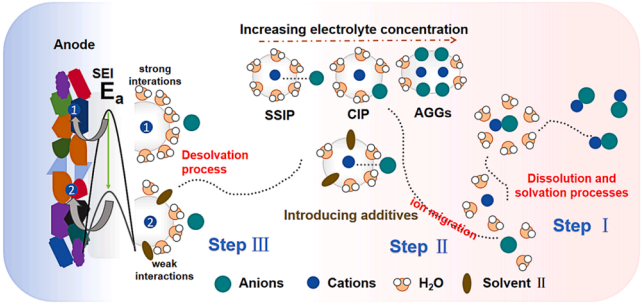

Fig. 4. Formation and evolution of solvated structures. The three steps of the solvation/de-solvation process and schematic diagrams of different solvation structures.

Interfacial dynamics is widely regarded as one of the important factors governing battery performance[95]. The interfacial processes include three key mechanisms: (1) ion de-solvation at the electrode interface, (2) ion transport across the electrolyte/electrode interface, and (3) interfacial charge transfer reactions. Particularly, cation de-solvation emerges as the rate-limiting step, with its free energy barrier exceeding that of cation diffusion through the SEI[96,97]. This de-solvation barrier is highly sensitive to both interfacial chemistry and electrolyte composition, making targeted interface design crucial for optimizing solvent removal from the solvation shell. For example, Li et al. [98]. accelerated the lithium de-solvation process by adjusting the composition of the electrolyte. At low temperatures, cation–solvent interactions are significantly intensified, leading to a more pronounced solvent-dominated solvation structure within the electrolyte. This temperature-dependent enhancement not only strengthens cation–solvent coordination but also increases the solvent coordination number, thereby elevating energy barrier for cation de-solvation at the molecular level. A higher solvation energy correlates with a greater de-solvation barrier[99]. Moreover, key electrolyte properties—including ionic conductivity, electrochemical stability window (ESW), thermal stability, and hydrolytic resistance—are highly related to the solvation structure of metal ions. This structure, defined by the interactions among metal ions, anions, and solvent molecules, forms a relatively stable solvation sheath that critically influences electrolyte performance.

2.2.3. *Solvation thermodynamics*

Solvation involves the formation of complexes among cations, anions and solvent molecules[101]. The following thermodynamic variables can be used to describe the solvation behavior of electrolytes.

Electrostatic potential (ESP), representing the surface charge distribution of molecules, plays a significant role in understanding various molecular behaviors and chemical reactivity[102]. Regions exhibiting highly negative electrostatic potential (ESP) demonstrate a strong affinity for cations, indicating that the strength of cation–anion interactions is closely linked to the extent of negative charge accumulation. In particular, the most negative ESP sites on anions serve as preferential coordination sites for cations and also reflect their binding affinity with surrounding water molecules. For aqueous zinc salts, the ESP-based affinity sequence is: $SO_4^{2-} > Ac^- > NO_3^- > Cl^- > BF_4^- > ClO_4^- > CF_3SO_3^- > TFSI^-$. Notably, SO_4^{2-} exhibits the most negative ESP value (−11.1 eV), facilitating the formation of Zn^{2+}– SO_4^{2-} clusters and thereby weakening Zn^{2+}–H_2O interactions(Fig. 5**a,b**). In contrast, Cl^- has a more uniform ESP distribution around its atomic nucleus with a value of −5.98 eV and shows reduced tendency for the aggregation of medium-concentration cations. While high negative ESP enhances cation attraction, it also increases anion–anion repulsion[94], necessitating careful consideration of competitive coordination effects when designing low-temperature electrolytes with multi-anion coordination solvation structures[103]. Generally, lower negative ESP values correspond to weaker cation binding, stronger cation–water interactions, more uniform charge distribution, and lower electrolyte freezing points. However, in general electrolytes containing BF_4^- and ClO_4^- have lower freezing points. This is mainly attributed to the interaction between BF_4^-

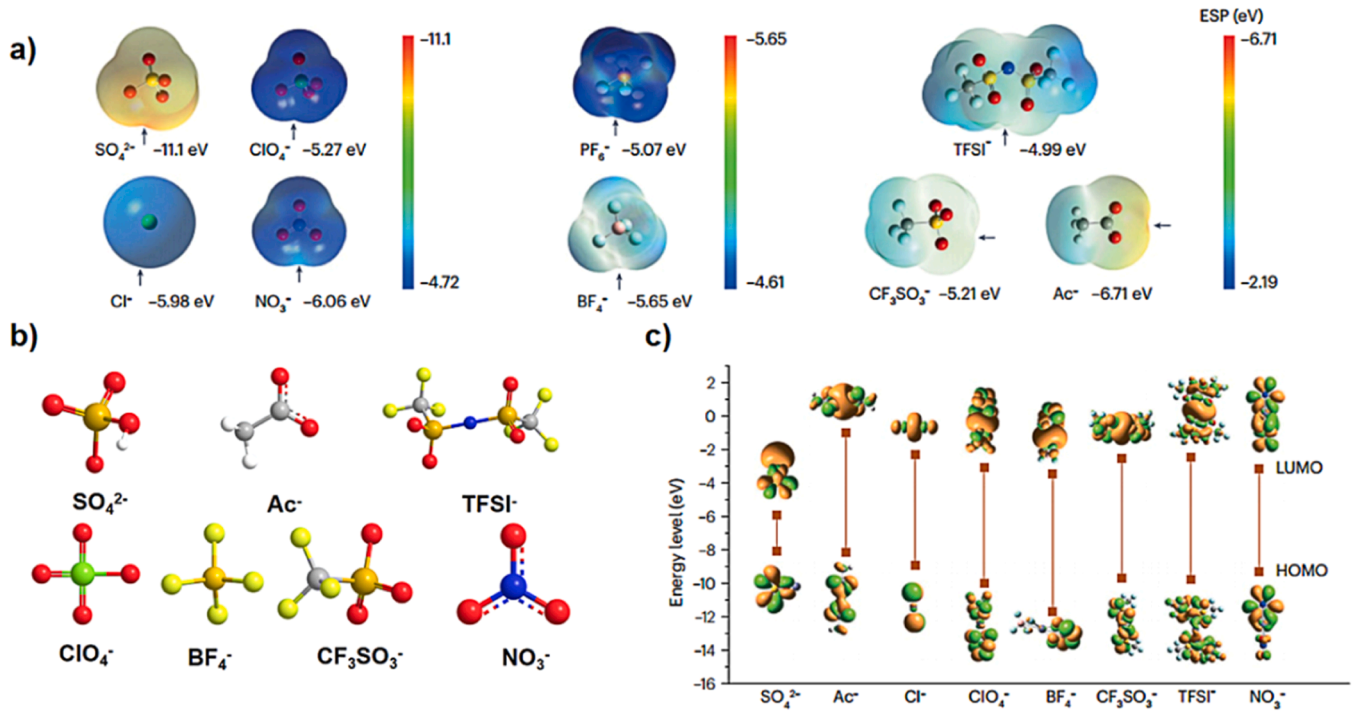

Fig 5. Thermodynamic descriptors. a) Electrostatic potential (ESP) [100]. b) Anion type. c) Highest occupied molecular orbital (HOMO) and lowest unoccupied molecular orbital (LUMO) [100].

and ClO_4^- and water. The strong hydrogen bond interaction formed between ClO_4^- and H_2O effectively disrupts the HB network between water molecules, thereby inhibiting the formation of ice crystals and lowering the freezing point[104]. The inherent four BF bonds of the BF_4^- anion can not only form O—H… F bonds with water, but also replace the H_2O molecules in the solvation structure of the zinc ion, weakening the interaction of the hydrogen bond network in the aqueous solution[105], thereby indicating that solvents with higher dielectric constants facilitate more favorable ion solvation processes.

3) The **highest occupied molecular orbital** (HOMO) and **lowest unoccupied molecular orbital** (LUMO) are commonly employed to qualitatively assess the electrochemical stability of salts. The electrochemical stability window (ESW) of an electrolyte is defined as the energy difference between the LUMO and HOMO levels[106]. Among various anions, BF_4^- exhibits the lowest HOMO energy(Fig. 5**c**), indicating superior intrinsic oxidation stability, while Ac^- possesses the highest LUMO energy, reflecting strong resistance to reduction. Thermodynamically, the HOMO of the electrolyte must lie below the cathodic reaction potential, and the LUMO above the anodic reaction potential. Although computational accuracy may be limited, molecular orbital analysis offers valuable insights into the electrochemical behavior of zinc salts and solvents[107]. Notably, changes in the solvation environment of Zn^{2+} can alter HOMO–LUMO characteristics, thereby influencing the oxidative and reductive stability of coordinating anions and solvent molecules.

In summary, the solvation behavior of electrolytes is governed by several key thermodynamic parameters. The electrostatic potential (ESP) distribution determines the strength of cation–anion interactions and modulates Zn^{2+}–H_2O coordination, thereby influencing freezing point depression. Solvation free energy ($\Delta G_{(sol)}<0$) reflects the spontaneity of solvation and is strongly correlated with the solvent's dielectric constant. The HOMO–LUMO energy gap serves as a qualitative measure of the electrochemical stability window, with specific anions (e.g., BF_4^- for oxidation resistance and Ac^- for reduction resistance) contributing to electrolyte stability through their orbital energy levels. Collectively, these variables provide a theoretical framework for the rational design of multi-anion coordination solvation structures aimed at enhancing the performance of aqueous electrolytes.

2.2.4. *Interactions between solvation structure components*

The solvation capacity depends on the strength of the cation-solvent (ion-dipole) interaction. In most electrolyte systems, anions tend to enter the solvation sheath through cation-anion (ion-ion) interactions, and the shielding effect of the solvent weakens this interaction. The competition between cationic-solvent and cation-anion interactions ultimately determines the final solvation structure. This fundamental understanding of the cationic solvation structure provides inspiration for designing multifunctional mixed solvent electrolytes for advanced batteries[108].

The increase in SSIP proportion at low temperatures is attributed to changes in interactions between electrolyte components. These interactions are fundamentally electrostatic in nature, comprising two dominant types: ion-ion interactions and ion-dipole interactions. According to classical physics, these forces can be defined as[109,110]:

$$U_{ion-ion} = -\frac{1}{4\pi\varepsilon} * \frac{Z_1 Z_2 e^2}{r}$$

$$U_{ion-dipole} = -\frac{1}{4\pi\varepsilon} * \frac{ze\mu\cos\theta}{r^2}$$

Here, U represents electrostatic potential energy, ε is the dielectric constant, ze represents the charge of ions, r is the distance, μ represents the dipole moment of solvent molecules, and θ represents the dipole angle. In electrolyte systems, cationic solvation structures emerge from a competitive equilibrium between cation-anion (ion-ion) and cation-solvent (ion-dipole) interactions. While temperature does not explicitly appear in the above equations, it indirectly governs solvation behavior through volumetric effect. When no phase change occurs, cooling reduces the electrolyte volume, thereby decreasing the average intermolecular distance (r), which amplifies both ion-ion and ion-dipole interactions according to their respective distance dependencies (r^{-1} and r^{-2}). Consequently, cooling preferentially enhances ion-dipole coupling ($U_{ion-dipole}$) over ion-ion interactions ($U_{ion-ion}$), promoting

greater solvent penetration into the primary solvation shell. This mechanistic understanding explains the observed low-temperature shift toward solvent-dominated coordination. It was found that the introduction of co-solvents with low dielectric constants, such as fluorine-based solvents or non-solvents, could mitigate this temperature-induced structural reorganization[111]. Meanwhile, it is worth noting that the dipole moment of the solvent is another factor determining the $U_{ion-dipole}$ value. At low temperatures, solvents with higher dipole moments exhibit stronger ion–dipole interactions, increasing their tendency to enter the cationic solvation sheath. Conversely, in systems where anions penetrate the inner solvation layer at low temperatures, this behavior may be attributed to the use of solvents with lower dipole moments [112,113]. A lower dipole moment results in a slower increase in $U_{ion-dipole}$ as temperature decreases, which may remain insufficient to surpass the rise in $U_{ion-ion}$. Therefore, incorporating low-dipole-moment solvents can moderate the temperature-induced changes in solvation structure by suppressing the growth of ion–dipole interactions, offering a strategic approach to stabilizing electrolyte behavior under low temperature conditions.

In summary, the low-temperature solvation structure is governed by the competitive balance between cation-anion (ion-ion) and cation-solvent (ion-dipole) interactions. Volume contraction of the electrolyte at low temperatures reduces intermolecular distances, which preferentially amplifies ion-dipole coupling (scaling as r^{-2}) over ion-ion interactions (r^{-1}), driving solvent penetration into the primary solvation shell. This temperature-dependent shift can be effectively mitigated through electrolyte engineering strategies employing low-dielectric-constant solvents (e.g., fluorinated compounds) or low-dipole-moment solvents to maintain the stability of the solvation structure.

3. Low-temperature optimization strategy

Electrolytes play a central role in battery systems by enabling the transport of charge carriers between the cathode and anode. In aqueous batteries, the temperature adaptability is closely linked to the thermal stability of the electrolyte, with freezing at sub-zero temperatures posing a major challenge to reliable operation under harsh conditions. To address this challenge, various strategies have been developed to suppress the chemical activity of water, including lowering the electrolyte's freezing point and optimizing cation solvation structures by displacing water molecules from the solvation sheath. This section provides a comprehensive overview of recent advances in electrolyte engineering aimed at enhancing the low-temperature performance of aqueous batteries.

3.1. Hydrogen bond network modulation

Water molecules serve as fundamental components of HB networks, exhibiting dual functionality as both hydrogen bond donors (HBD) and acceptors (HBA) according to Lewis acid-base theory[114]. In electrolytes, water molecules exist in three distinct HB environments:(1) tetrahedrally coordinated "blocky" H_2O (4 HBs), (2) partially connected H_2O clusters (1–3 HBs), and (3) isolated H_2O molecules (HB-free). As temperature decreases, the kinetic energy of water molecules is reduced, which promotes the formation of highly ordered HB networks. This structural ordering is a key factor leading to electrolyte freezing, thereby compromising the low-temperature performance of aqueous battery systems. Consequently, disrupting the formation of these ordered HB networks is essential—not only for depressing the freezing point of the electrolyte but also for suppressing hydrolysis reactions.

Current strategies for regulating HB networks in aqueous electrolytes can be broadly categorized into four approaches (Fig. 6). (a) Anion regulation: it involves selecting anions with varying binding affinities to water or distinct HB acceptor elements (e.g., N, F, O) to modulate water activity. Incorporating structure-breaking anions from the Hofmeister

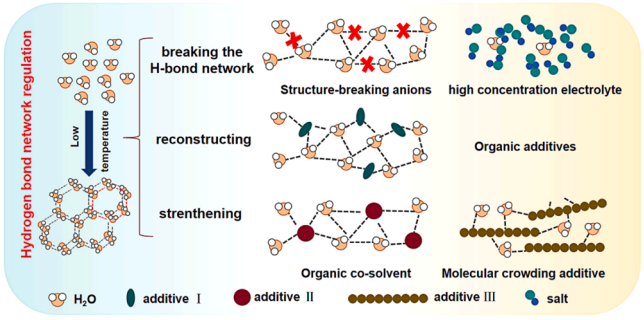

Fig. 6. Low-temperature optimization strategy based on hydrogen bond network regulation.

series into high-concentration electrolytes can effectively disrupt HB networks. (b) Additive introduction: it employs low-freezing-point, low-viscosity additives that interact with water to weaken HB clusters. For example, additives composed solely of HB acceptors with high Gutmann donor numbers (DN) can reconstruct the HB network and inhibit proton transfer via the Grotthuss mechanism[115]. (c) Co-solvent strategy: it enhances HB network regulation by introducing dipolar co-solvents that create a molecularly crowded environment, increasing system entropy and impeding the formation of low-entropy HB structures. (d) Eutectic electrolyte design: it reshapes the HB network to reduce molecular ordering and significantly lower the freezing point of water, thereby improving low-temperature performance.

3.1.1. Anion modulation

Since it was first demonstrated in 1934 that ions can disrupt the HB network among water molecules[116], ion-induced modulation of water's tetrahedral structure has remained a central research focus. Ions with high charge density and small ionic radii exhibit strong electrostatic interactions with water, which thermodynamically lowers the enthalpy change (ΔH) and enhances the electrolyte's low-temperature performance. Anions, acting as HBD or HBA, can also coordinate with water molecules, thereby disrupting the original HB network and effectively depressing the freezing point of the electrolyte.

As illustrated in Fig. 7**c**, the electrostatic surface potential (ESP) and water-binding energies of anions in various zinc salt aqueous electrolytes—such as $ZnSO_4$, $Zn(NO_3)_2$, $ZnCl_2$, ZnI_2, and $Zn(OTf)_2$—demonstrate their influence on HB dynamics and freezing point depression [11]. HB analysis reveals a progressive reduction in the number of HB per H_2O molecule from $ZnSO_4$ to $Zn(OTf)_2$, corresponding to a freezing point decrease from –9.8 °C to –34.1 °C. This structural disruption can enhance low-temperature electrochemical performance of the aqueous electrolytes. The ClO_4^--based electrolyte further exemplifies this effect, offering both anti-freezing properties and high ionic conductivity[119]. Without the addition of any organic additives, a 3 M $Zn(ClO_4)_2$ aqueous solution also achieves a high ionic conductivity of 4.23 mS cm^{-1} at an ultra-low temperature of –50 °C[104], as shown in Fig. 7**b** Spectral characterization and molecular dynamics (MD) simulations (Fig. 7**d**) [104] confirm that ClO_4^- disrupts H_2O–H_2O hydrogen bonds while forming new HBs with water, restoring dynamic equilibrium and lowering the freezing point. Statistical analysis (Fig. 7**a**)[104] shows that the number of anion–H_2O hydrogen bonds increases from 4 in 3 M $ZnSO_4$ and 3 in 3 M $Zn(CF_3SO_3)_2$ to 9 in 3 M $Zn(ClO_4)_2$, indicating the superior ability of ClO_4^- to restructure the HB network and enhance low-temperature electrolyte performance[120]. The aqueous potassium-ion battery composed of 10 m KCF_3COO electrolyte with a large degree of hydrogen bond breaking also has good low-temperature performance[121]. Additionally, incorporating anions with highly electronegative elements—such as N, O, and F—as HB acceptors is an effective strategy for low-temperature electrolyte design by modulating water structure. Particularly, the tetrafluoroborate anion (BF_4^-),

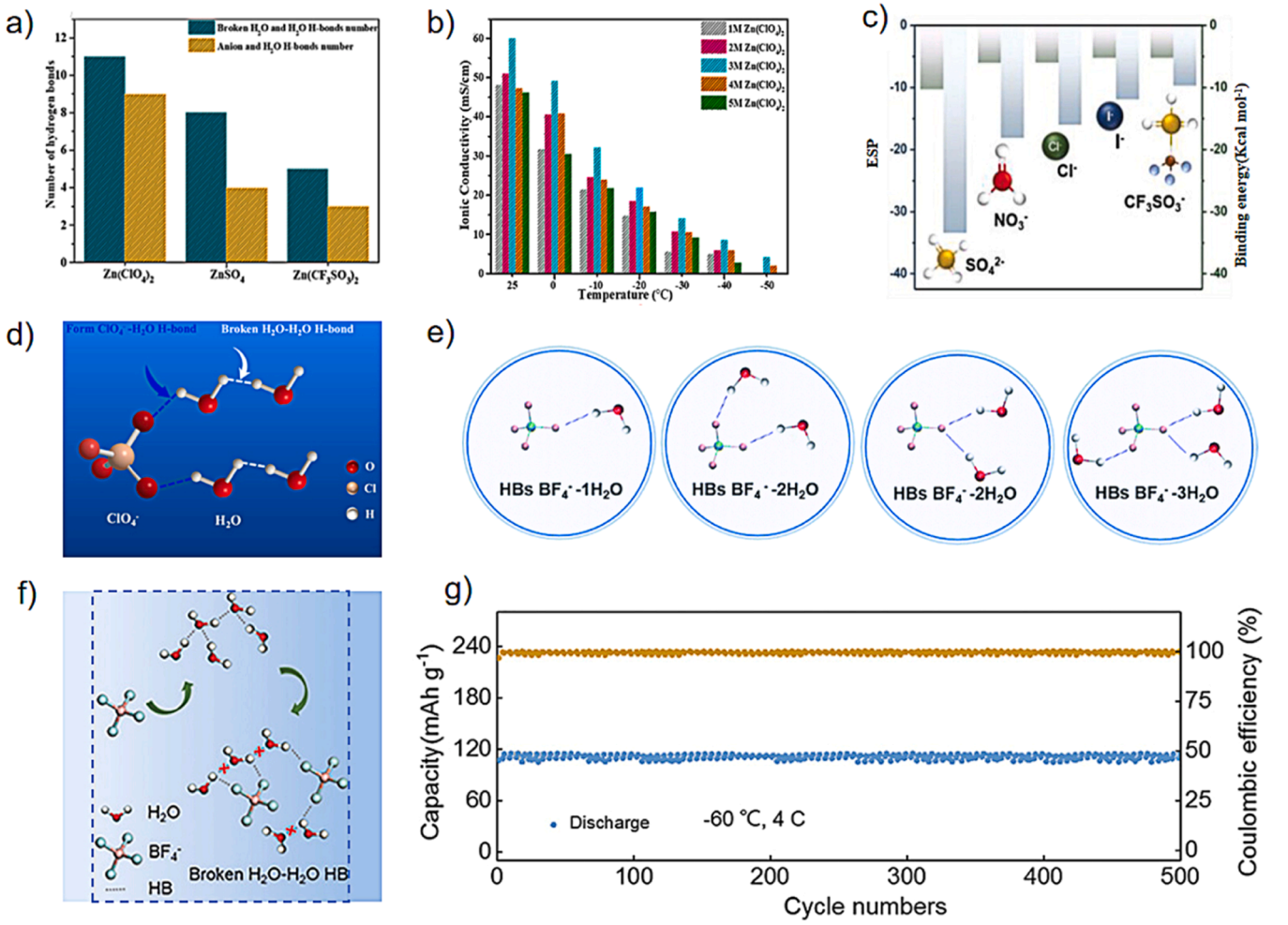

Fig. 7. Anion regulation: a) Average hydrogen bond number of $Zn(ClO_4)_2$, $ZnSO_4$ and $Zn(Cf_3SO_3)_2$ systems [104]. b) Comparison of ionic conductivity of $Zn(ClO_4)_2$ aqueous solutions of different concentrations at different temperatures [104]. c) ESP of different selected anions and their binding energy with H_2O [11]. d) Schematic diagram of the possible mechanism by which perchlorate anion interaction affects hydrogen bonds in $Zn(ClO_4)_2$ aqueous solution [104]. e) Types of hydrogen bonds present in BF_4^- solution [117]. f) BF_4^- breaks the hydrogen bonds between water molecules [118]. g) Battery performance [118].

containing four fluorine atoms, readily forms weak O–H···F hydrogen bonds with water molecules (Fig. 7**f**)[118]. MD simulations (Fig. 7**e**) reveal four distinct HB types between BF_4^- and water in a 4 M $Zn(BF_4)_2$ aqueous solution[117]. Each BF_4^- anion can coordinate with up to three water molecules, forming a $Zn(H_2O)_4(BF_4)_2$ solvation structure. This tailored solvation environment enables Zn//δ-MnO_2 cells using Zn $(BF_4)_2$ electrolyte to maintain stable capacity even at –60 °C (Fig. 7***g***), highlighting the potential of fluorinated anions in enhancing low-temperature battery performance[117].

In general, the effectiveness of anions in suppressing water activity within electrolytes is constrained by their solubility and coordination capacity. Highly soluble, hydrophilic anions—such as NO_3^-, BF_4^-, OTf^-[122], bis(trifluoromethylsulfonyl) imide ($TFSI^-$)[123], F^-, and ClO_4^- —possess abundant hydrogen bond donor/acceptor (HBD/HBA) sites and are widely employed in high-concentration electrolytes to suppress water activity[124]. In such systems, anions such as $TFSI^-$, Cl^-, and F^- form stable HB networks with water molecules, effectively "locking" them in place and disrupting intermolecular H_2O–H_2O hydrogen bonding. This interaction lowers the chemical activity of water and suppresses its tendency to form an ordered HB network. Simultaneously, nearly all water molecules are strongly coordinated with cations and confined within their solvation shells, resulting in a complete breakdown of the intermolecular HB network among water molecules. This dual effect contributes to the significantly reduced freezing point observed in high-concentration electrolytes, thereby enhancing their suitability for low-temperature battery applications. For instance, a $Li_3V_2(PO_4)_3$//$LiTi_2(PO_4)_3$ battery using 21 m (mol kg^{-1}) LiTFSI electrolyte delivers a reversible capacity of 111 mAh g^{-1} at –20 °C, retaining 92.5 % of its capacity at 25 °C[123]. Similarly, saturated LiCl electrolytes enable $LiCoO_2$ electrodes to maintain ~72 % of its room-temperature capacity at –40 °C[125]. Given the cost and concentration requirements of such systems, the concept of locally high-concentration electrolytes has been proposed. In these systems, the hydrophobic nature of $TFSI^-$ promotes preferential hydrogen bonding between water and cations (e.g., Li^+), rather than with $TFSI^-$ itself. This competitive coordination creates localized high-concentration zones around cations, further weakening the bulk HB network and enhancing low-temperature stability.

In summary, anion regulation strategy is primarily applied to conventional dilute electrolyte systems, offering advantages such as high ionic conductivity, low viscosity, and cost-effectiveness. However, its applicability is constrained by the limited selection of salts that meet anti-freezing requirements, resulting in a relatively narrow operational temperature range. In contrast, high-concentration electrolyte systems significantly extend the usable temperature range into ultra-low regions, while also broadening the electrochemical stability window and suppressing cathode dissolution. Nevertheless, these systems face challenges including increased viscosity, crystallization and precipitation risks, reduced ionic conductivity, and higher material costs, which collectively hinder their scalability for practical applications.

3.1.2. Additive introduction

The incorporation of trace amounts (typically <10 % by weight, molar, or volume) of organic or inorganic substances into aqueous electrolytes—commonly referred to as additives—can effectively suppress ice crystallization, thereby lowering the freezing point and enabling low-temperature operation of water-based batteries. Organic additives interact with water molecules via HBA/HBD groups, disrupting the original HB network and forming a new stabilized additive–-water HB network. This reconstructed structure effectively inhibits the formation of continuous HB network among freely mobile water molecules, thus suppressing ice crystallization. The effectiveness of organic solvents in controlling the water–ice phase transition is governed by their intrinsic properties, including polarity, freezing and boiling points, dielectric constant, and concentration. In contrast, inorganic additives achieve similar freezing point depression by modulating the proportion of strong HBs within the electrolyte.

For example, the polyhydroxy organic compound 1,4-dioxane-2,5-diol (DOL) forms strong HBs with water molecules (Fig. 8**b**), disrupting the native weak HB network among free water molecules (Fig. 8**c**) and effectively regulating free water content. An electrolyte containing 100 mM DOL maintains high ionic conductivity (20.86 mS cm^{-1}) at −10 °C, whereas the DOL-free counterpart freezes[126]. To achieve optimal coordination with water molecules, the solvent–water binding energy must exceed that of water–water interactions. Similarly, in order to effectively converts active water molecules in the solvation shell to less reactive bulk water by adding DOL, the binding energy between DOL and zinc needs to be greater than that between zinc and water molecules.(Fig. 8**a**). Inspired by the molecular crowding effect in biological systems, which reduces free H_2O activity, small-molecule crowding environments can similarly disrupt HB structures[130]. Additives that induce molecular crowding reduce free water content, suppress hydrogen evolution reactions (HER), and lower the freezing point. For instance, hydroxyl-rich galactomannan polysaccharides (q-GPA), capable of inducing such effects, enable battery operation at −30 °C. A q-GPA-modified Zn–$Na_2V_6O_{16}\cdot 1\cdot 5H_2O$ (NVO) full cell demonstrates exceptional low-temperature performance, with 99.2 % capacity retention over 5000 cycles at −30 °C. Mechanistic studies (Fig. 8**f**) reveal that the polyhydroxy galactomannan framework reconfigures the HB network, significantly reducing water activity and inhibiting ice formation below zero degrees[127]. At low temperatures, the original HB network (Fig. 8**d**) readily transitions into an ice lattice, but q-GPA disrupts this structure through strong interaction between q-GPA and water. By balancing HB and ionic interactions, electrolytes with critical q-GPA concentrations remain functional at subzero temperatures. In-situ variable-temperature FTIR spectroscopy confirms that, unlike the Zn $(OTf)_2$ electrolyte, the $Zn(OTf)_2$–q-GPA system maintains stable O–H stretching vibrations across −30 to 30 °C (Fig. 8**e**), further validating q-GPA's role in structural regulation and ice suppression. In addition to

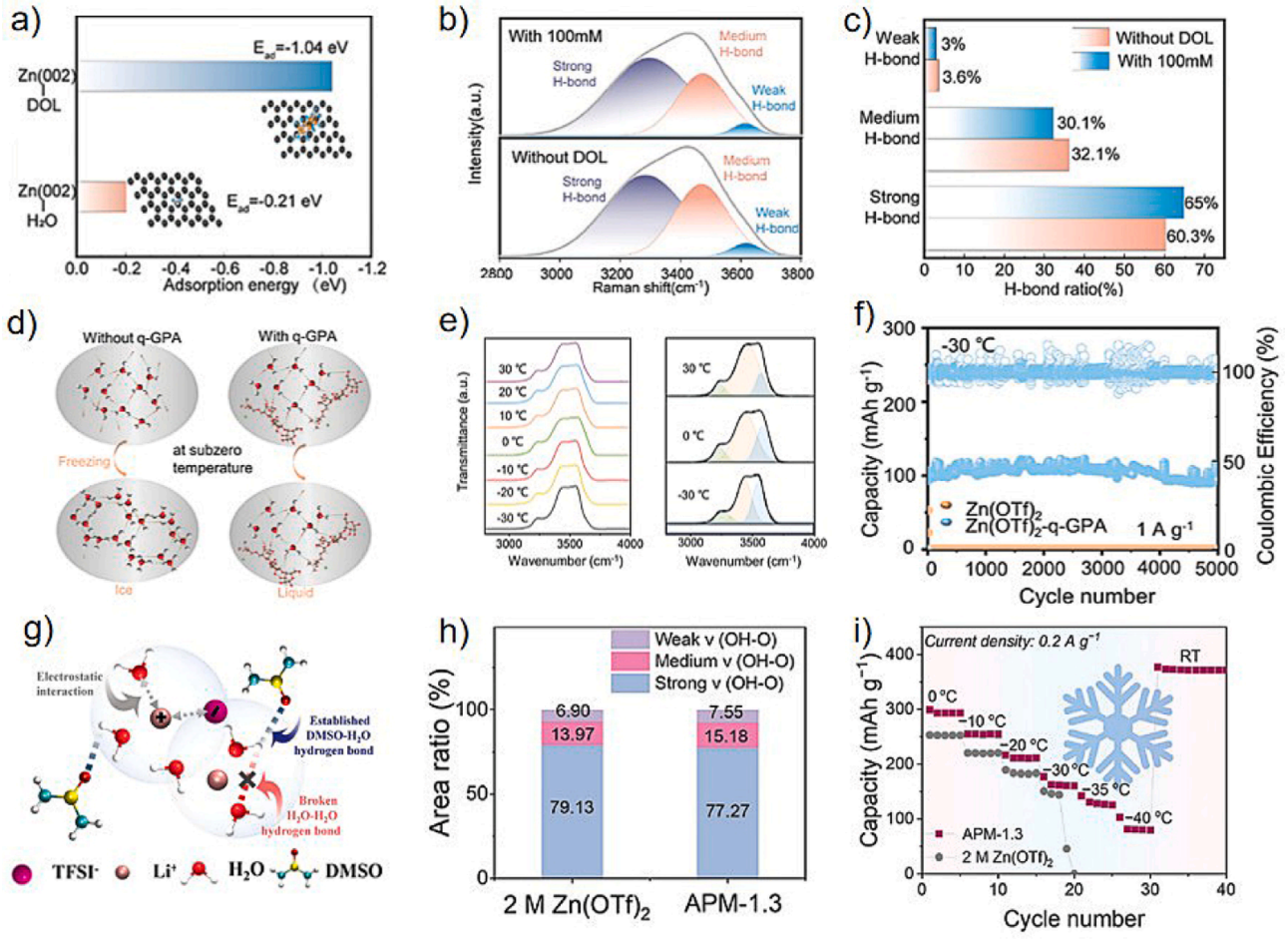

Fig. 8. Additive: a) H_2O and DOL on the Zn (002) crystal surface [126]. b) The Raman spectra of the strong, medium and weak hydrogen bond vibration regions were fitted [126]. c) Comparison of strong, medium and weak hydrogen bond contents [126]. d) Schematic diagram of the original hydrogen network between water molecules with q-GPA at low temperatures [127]. e) In-situ variable-temperature FTIR spectra of the typical O—H tensile vibration mode of $Zn(OTf)_2$-q-GPA electrolyte within the range of 30 to −30 °C [127]. f) The influence of $Zn(OTf)_2$ and $Zn(OTf)_2$-q-GPA electrolytes on the cycling performance of Zn//NVO batteries [127]. g) Schematic diagram of possible supramolecular interactions among LITFSI, DMSO and water [128]. h) Area ratio of strong, medium and weak HBs of H_2O molecules [129]. i) Cycling stability [129].

hydrophilic hydroxyl groups, dimethyl sulfoxide (DMSO, $(CH_3)_2SO$) is widely employed as a low-temperature additive due to its high polarity, elevated boiling point, and excellent thermal stability. As a sulfur-containing compound, DMSO functions exclusively as a HBA in mixed DMSO–H_2O systems[131], owing to the two lone electron pairs on the oxygen atom of the sulfoxide group. In this configuration, water molecules act as HBDs, reconstructing the original H–O···H HB network into a new structure characterized by $S=O\cdots$H–O interactions (Fig. 8**g**) [128]. This restructured network significantly depresses the freezing point, allowing the electrolyte to remain in a liquid state down to −40 °C. In addition, the electrolyte obtained by adding DMSO to a 2 M $NaClO_4$ aqueous solution achieved the performance of an ionic conductivity of 0.11 mS cm^{-1} even at an ultra-low temperature of −50 °C [132].

Inorganic additives such as calcium chloride ($CaCl_2$) and heteropoly acids (e.g., ammonium phosphomolybdate, APM) also serve as effective low-temperature modifiers. $CaCl_2$ interacts strongly with water molecules, altering the HB distribution within the electrolyte and thereby lowering its freezing point[120]. When incorporated into an optimized electrolyte formulation (3.86 m $CaCl_2$ + 1 m $NaClO_4$), an all-inorganic $Na_2CFe(CN)_6$//activated carbon battery achieves a high discharge capacity of 74.5 mAh g^{-1} at 1 C and demonstrates ultra-stable cycling performance over 6000 cycles at −30 °C and 10 C. Additionally, the inclusion of APM in $Zn(OTf)_2$-based electrolytes attenuates water–water interactions, decreasing the proportion of strong HBs while increasing the fraction of weaker ones (Fig. 8**h**). As the temperature drops from 0 °C to −40 °C, the APM-1.3 electrolyte maintains superior cycling stability and capacity (Fig. 8**i**). Upon returning to room temperature, the specific capacity of the APM-1.3 electrolyte is largely restored, highlighting its reversible structural modulation and robust low-temperature performance[129]. Some "non-conventional" electrolyte additives such as graphene oxide quantum dots have also been proven to effectively inhibit the growth of ice crystals[133].

In summary, the incorporation of additives into aqueous electrolytes effectively weakens intermolecular interactions among H_2O molecules, reduces the proportion of strong HBs, and enhances ionic conductivity. Additionally, additive adsorption on the electrode surface contributes to a more uniform electric field distribution, promoting homogeneous zinc ion deposition while suppressing dendrite formation and corrosion. Future research should focus on the synergistic regulation of the electrolyte's operational temperature window and the protective mechanisms at the zinc anode interface, aiming to further improve the long-term cycling stability of aqueous zinc-based batteries.

3.1.3. Co-solvent strategy

A key requirement for co-solvents in aqueous electrolytes is their miscibility with water. The introduction of the organic co-solvent and molecular crowding agents can effectively establish a HB network within the electrolyte. Such substances (e.g., sulfone sulfolane (SL)[12], succinonitrile (SN)[134], acetonitrile (AN)[135], acetone[136], urea [137], etc.) usually contain highly polar functional groups that enable strong dipole-dipole interactions with water molecules. The higher the binding energy between additive molecules and free water molecules, the stronger the HB force established[138]. By forming a dense HB network, these additives can transform water molecules that are originally in a long-range ordered and freely moving state into a localized bound state. This microstructure transformation significantly reduces the freezing point of aqueous electrolytes[139]. Moreover, the introduction of substantial amounts of co-solvent increases the entropy value of the entire electrolyte system, thereby synergistically hindering the transition of the system to a low-entropy solid state.

Alcohols, due to their abundant hydroxyl groups, establish a strengthened HB network with free water molecules[142]. Among them, polyethylene glycol (PEG 200) has shown remarkable effects in improving the low-temperature performance of aqueous electrolytes due to its unique molecular structure. Studies reveal that the ether oxygen atoms (C—O-C) in PEG 200 possess a higher negative charge density than the O atoms in H_2O[143], resulting in weaker HBs between PEG and water (bond energy ≈ −0.072 eV; bond length ≈ 2.26 Å) compared to the stronger water–water HBs (bond energy ≈ −0.199 eV; bond length ≈ 1.8 Å), as shown inFig. 9**a**[140]. As a HBA, PEG forms a global weak hydrogen bond with H_2O when introduced as co-solvent [140]. In particular, the incorporation of PEG 200 into a 2 m $ZnCl_2$ aqueous electrolyte enables battery operation at extremely low temperatures, down to −40 °C. This enhanced anti-freezing performance is closely linked to the ability of co-solvent to modulate the local environment of water molecules. Differential scanning calorimetry (DSC) analysis (Fig. 9**b**) demonstrates that increasing the concentration of PEG 200 significantly lowers the freezing point of the electrolyte. Notably, the molecular weight of PEG plays a critical role in its ability to suppress free water activity. Low-molecular-weight PEGs, such as PEG 100, possess shorter chain lengths that are insufficient for effectively encapsulating water molecules, resulting in limited inhibition of water crystallization. In contrast, the optimized PEG co-solvent system exhibits superior anti-freezing performance, attributed to its enhanced capacity to regulate the water molecule environment and disrupt long-range HB network. Conductivity measurements (Fig. 9**c**) reveal that all electrolytes exhibit a similar decline in ionic conductivity as the temperature decreases from 30 °C to 0 °C. However, below 0 °C, mixed electrolytes containing PEG demonstrate significantly higher conductivity compared to the pure 2 m $ZnCl_2$ system. Notably, the optimized 7:3 hybrid electrolyte maintains an ionic conductivity of 5.6×10^{-5} S cm^{-1} at −40 °C, whereas the $ZnCl_2$-only electrolyte drops sharply to 2×10^{-7} S cm^{-1}. This superior physicochemical stability directly endows enhanced battery performance under extreme low-temperature conditions.

Beyond PEG, other types of organic co-solvents also effectively improve the low-temperature behavior of electrolytes through different mechanisms. As the lightest nitrile organic solvent by molar mass, acetonitrile (AN) is widely used due to its high miscibility with water and low freezing point. The -C≡N group in its molecule can act as a HBA and electrostatically interact with the hydrogen atoms in water that act as HBD, thereby reconstructing the HB network around the water molecule[144]. For instance, the introduction of AN as a co-solvent into a conventional high-concentration (21 m) LiTFSI electrolyte results in the formation of an "acetonitrile/water-in-salt" (AWIS) electrolyte. At an optimal concentration of 5 m, the AWIS system exhibits markedly improved physicochemical properties, including enhanced ionic conductivity, reduced viscosity, and a lowered freezing point compared to the original 21 m water-in-salt (WIS) electrolyte. Importantly, the wide electrochemical stability window of the electrolyte is preserved, and its operational temperature range is extended down to −30 °C[145]. Similarly, formylamine (FA), a highly polar solvent, has been reported to improve the low-temperature behavior of aqueous sodium-ion batteries [141]. FA contains both HBA (carbonyl $C=O$) and HBD (amino –NH_2) groups, enabling coordination with the hydroxyl groups of water to form H_2O–FA clusters. This coordination effect effectively inhibits the formation of water clusters with tetrahedral HB structures between water molecules, significantly altering the chemical environment of water molecules. The vibration evolution is shown in Fig. 9**d** [141]. In the optimized mixture, both the carbonyl stretching vibration and the amine bending vibration of FA move towards the higher wave-number side, confirming the change in the intermolecular interaction[146]. Consequently, the freezing point of the electrolyte drops below −50 °C. These improvements highlight the potential of co-solvent engineering in advancing the low-temperature performance of aqueous battery systems.

3.1.4. Eutectic electrolyte design

The formation of deep eutectic electrolytes (DES) arises from the intricate coordination of interactions among metal salts, ligands, and additives[147,148]. These systems exhibit eutectic points significantly lower than those of their individual components and even below the

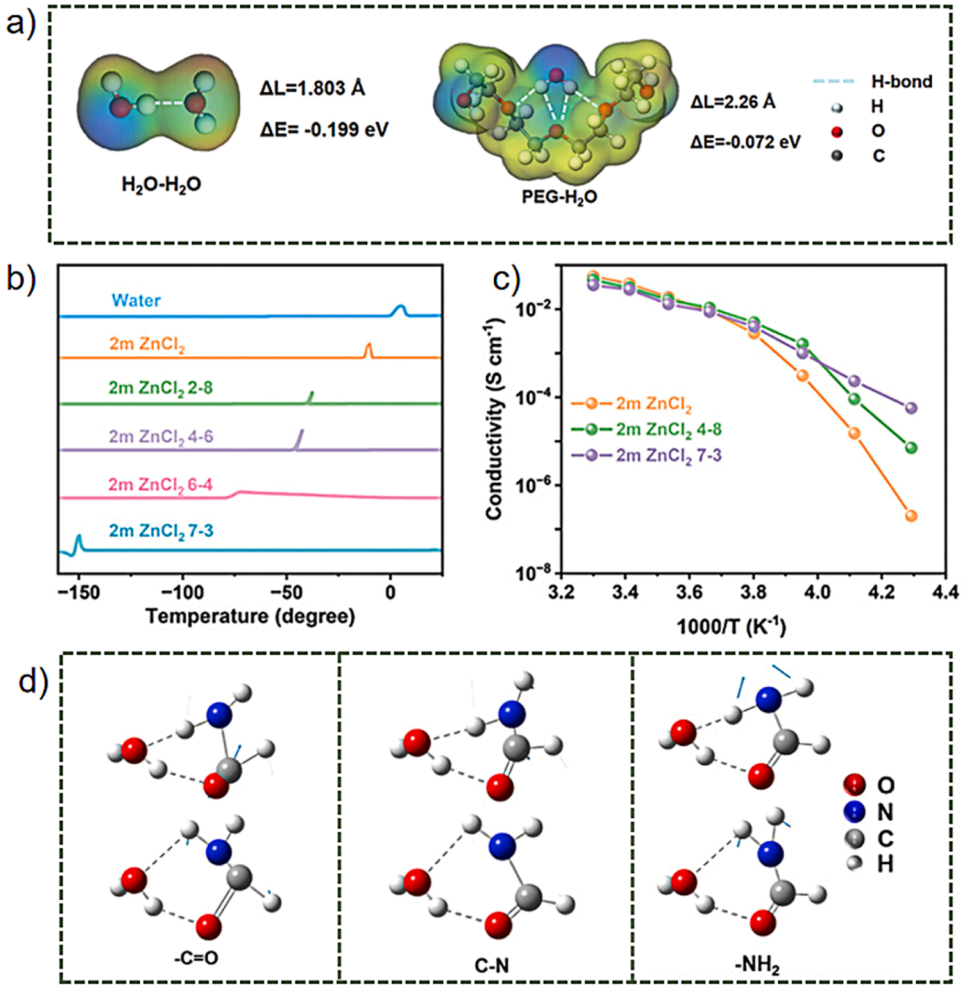

Fig. 9. Co-solvent: a) Schematic diagram of hydrogen bond interaction between PEG and water molecules [140]. b) Freezing point data obtained from DSC curves [140]. c) Ionic conductivity of mixed electrolytic substances at different temperatures [140]. d) Vibration evolution of different functional groups in the H_2O-FA cluster calculated by QC in the optimization scheme [141].

theoretical values predicted for ideal mixtures, indicating a strong negative deviation ($\Delta T_2 > 0$), as shown in Fig. 7**a**[149]. This pronounced depression in melting point makes DES highly suitable for antifreeze electrolyte applications. The bifunctional nature of DES plays a pivotal role in disrupting the original HB network among water molecules[150]. Specifically, the HBA components in DES interact with hydrogen atoms of water as HBD, while the HBD components form additional HBs with the oxygen atoms in water as HBA, collectively reconstructing the HB architecture and enhancing low-temperature stability[149]. This dual interaction mechanism allows DES to act as an efficient "HB disruptor", reshaping the HB network, reducing molecular order, and significantly lowering the freezing point of the electrolyte. Moreover, by weakening strong HBs, DES also mitigates water decomposition at elevated temperatures—such as suppressing the hydrogen evolution reaction (HER)—thereby broadening the electrolyte's electrochemical stability window. Additionally, DES systems are often environmentally benign, further supporting their application in sustainable energy storage technologies.

Based on the above mechanism, various DES systems have been developed to enhance the low-temperature performance of aqueous batteries. For example, acetylpropionic acid (AEV), which contains two dipolar groups (–COOH and $–C=O$), serves as an effective HBA, disrupting the original HB network by forming enhanced HB interactions with water molecules [150]. In a DES-x electrolyte composed of x vol % AEV, (1–x) vol % water, and 2 M $ZnSO_4$, the freezing point is significantly reduced. This is attributed to both dipole–dipole interactions between AEV and H_2O and dipole–ion interactions between AEV and Zn^{2+}, which collectively reshape the HB network (Fig. 10**e**) [151]. At an optimal composition of 50 vol % AEV (DES50), the electrolyte exhibits excellent ionic conductivity (Fig. 10**d**) and outstanding low-temperature performance. Specifically, a Zn//Zn symmetric cell demonstrated stable cycling for over 720 h at −20 °C under 0.25 mA cm^{-2} and 0.25 mAh cm^{-2} (Fig. 10**c**), while a full cell achieved nearly 650 h of deep cycling at 80 % depth of discharge (DOD) (Fig. 10**b**). Similarly, a mixed electrolyte containing 40 vol % ethylene glycol (EG) in 2 m $ZnSO_4$ retains high ionic conductivity (6.9 mS cm^{-1}) at −40 °C [152], facilitated by enhanced HB between EG and water (Fig. 10**f**). Furthermore, the polyeutectic electrolyte HEE30, composed of $Al(OTf)_3$, glycerol (Gly), β-sodium glycerophosphate pentahydrate (SG), and water in a 1:8:1:30 ratio, exhibits a significant shift towards a higher wavenumber of the H–O bending vibration peak (1600–1700 cm^{-1}) in FTIR spectra compared to the base electrolyte (Fig. 10***g***), confirming reduced water activity[153]. The unique eutectic network formed in HEE30 strengthens the HB between Gly and H_2O, thereby lowering the freezing point of the electrolyte (Fig. 10**h**), expanding the electrochemical window, and suppressing the HER[153].

In summary, strategies such as anion type modification, high-concentration salt formulation, incorporation of HBA/HBD-rich additives, and the design of eutectic electrolytes have proven effective in disrupting the original HB network and regulating the types of HB. These

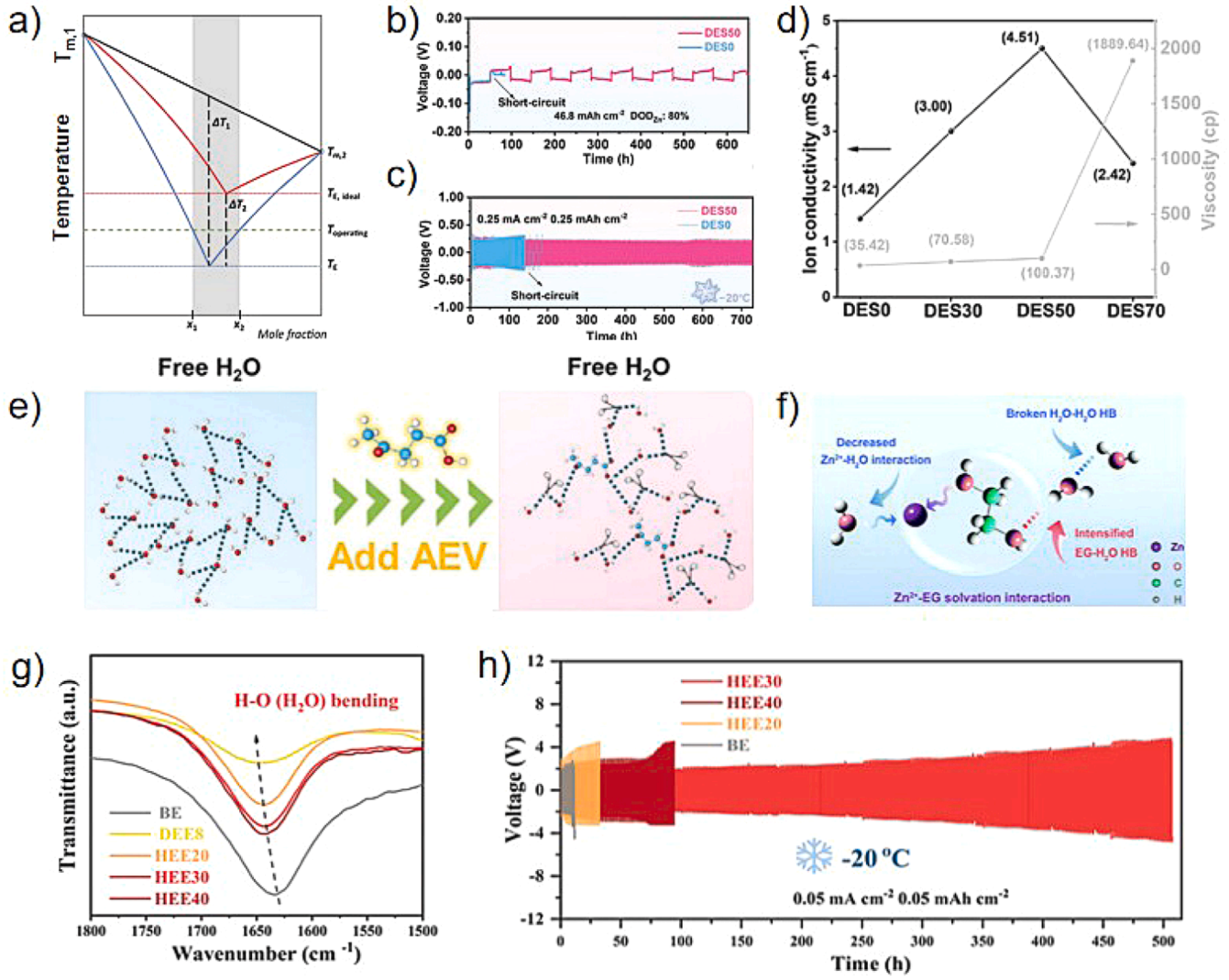

Fig. 10. Eutectic electrolyte: a) simple ideal eutectic mixture (red line) and deep eutectic mixture (blue line) [149]. b) The cycling performance of symmetrical zinc cells when the zinc utilization rate (ZUR) is 80 % [151]. c) Cycling performance of Zn//Zn symmetrical cells at −20 °C (0.25 mA cm^{-2} and 0.25 mAh cm^{-2}) [151]. d) The ionic conductivity and viscosity of DES-X electrolyte [151]. e) Schematic diagram of different behavioral characteristics of water molecules in aqueous solutions with or without AEV addition [151]. f) Schematic diagram of possible mechanisms by which the solvation interaction of Zn_2-EG affects the chemical properties of hybrid electrolytes [152]. g) Different water contents of electrolytes between 1500 and 1800 cm^{-1} The FTIR spectrum [153]. h) Cycling performance of Al/Al symmetrical cells using BE and HEE30 electrolytes at 0.05 mA cm^{-2} and 0.05 mAh cm^{-2} at −20 °C [153].

modifications inhibit the phase transition of water from liquid to solid, thereby lowering the freezing point of aqueous electrolytes. A key aspect of optimizing high-concentration salt electrolytes lies in reducing the structural order of the HB network in H_2O and modulating the HB coordination between anions and water molecules. However, the limited availability of HBAs (anions) in high-concentration systems means that reducing salt concentration can significantly impair electrolyte regulation. In contrast, additives—often rich in HBA/HBD functional groups—can exert substantial influence on the hydrogen evolution reaction (HER) and freezing behavior even at low concentrations. Future research should focus on integrating multiple approaches—combining the benefits of additives, high-concentration electrolytes, and eutectic systems—to develop advanced electrolytes with broad low-temperature operability and high safety.

3.2. Solvation structure design

The solvation structure of an electrolyte plays a pivotal role in determining its electrochemical stability, interfacial behavior, and overall battery performance. Modulating this structure can alter the highest occupied molecular orbital (HOMO) and lowest unoccupied molecular orbital (LUMO) levels of the solvent, thereby enhancing both its oxidative and reductive stability. The transport, deformation, and desolvation dynamics of solvated species—within both the bulk phase and at the electrode interface—are governed by intermolecular interactions and are critical to battery operation under low-temperature conditions. These processes are influenced by the competitive interactions among cations, anions, and solvent molecules that constitute the solvation structure. Consequently, extensive research has focused on designing intermolecular interactions in solvated structures to enhance low-temperature performance by exploring the charge transfer process at the molecular level.

3.2.1. Salt selection

The solvation structure of aqueous electrolytes is primarily governed by the relative strengths of cation–anion and cation–solvent interactions. When the interaction between cations and anions exceeds that between cations and solvent molecules, anions can partially replace solvent molecules within the solvation shell. This substitution alters the physicochemical properties of electrolytes and can be strategically

controlled through two main approaches: selecting different zinc salts or adjusting their concentrations. These methods enable precise tuning of the solvation environment, which is critical for optimizing electrochemical stability and enhancing battery performance, particularly under low-temperature conditions.

The physicochemical properties of anions, such as ionic size[157], asymmetry, hydrophobicity[158], position in the Hofmeister series [159], alongside the characteristics of cations, jointly exert a decisive influence on the solvation structure of the electrolyte. Anions, typically derived from salt dissociation, play a central role in shaping the solvation environment through their interactions with cations[160–162]. Strong anion-cation interactions lead to the formation of ion pairs, which in turn slow down the migration rate of cations. These ion pairs can further aggregate into ion clusters, resulting in compact solvation shells around cations and significantly increasing the de-solvation energy barrier of cations. As illustrated in Fig. 11**a**, the electrostatic potential (ESP) values of anions reflect their binding tendencies[154]. Additionally, the dissolution of different zinc salts alters HB interactions and pH levels, thereby affecting the stability and solvation structure of the electrolyte (Fig. 11**c**)[155] . Generally, anions with higher electronegativity and smaller ionic radii exhibit stronger binding affinities towards cations. Therefore, selecting or designing anions that weaken strong interactions between ions and optimize the solvation structure (i.e., reducing the formation of compact ion pairs or clusters) is an effective strategy to lower de-solvation barriers and enhance ion transport kinetics, particularly under low-temperature conditions.

Increasing salt concentration can effectively reduce the likelihood of contact between cations and water molecules, thereby enhancing cation–anion interactions and promoting the formation of a distinct cation coordination environment[163]. Additionally, reducing water content in aqueous electrolytes can effectively suppress parasitic reactions at the electrode interface, which are typically driven by highly active solvent molecules[164]. High-concentration "water-in-salt" (WIS) electrolytes induce the formation of unique solvation structures by significantly increasing the salt concentration and limiting the water content, In such electrolytes, the number of free water molecules is significantly reduced, while the anion-water HB pairings becomes widespread. And anions directly participate in cation coordination, forming contact ion pairs CIP and aggregates AGG[165]. This solvation sheath dominated by anions and a small amount of water molecules[166] has a relatively low de-solvation energy barrier and thus facilitate the formation of a stable, inorganic-rich solid electrolyte interface (SEI) layer [167]. Zinc ions (Zn^{2+}) are selected to serve as a representative case for studying cation solvation in aqueous electrolytes. In dilute solutions, strong electrostatic interactions between Zn^{2+} and polar water molecules form a well-defined $[Zn(H_2O)_6]^{2+}$ solvation sheath[168]. However, at elevated $ZnCl_2$ concentrations (e.g., 7.5 m), anions partially replace water in the primary solvation shell, forming mixed $[Zn(anion)_m(H_2O)_n]$ clusters [169]. This structural reorganization enables aqueous zinc-ion batteries (ZIBs) to operate at ultra-low temperatures (Fig. 11**b**), though high salt concentrations introduce trade-offs, including increased viscosity, reduced ionic conductivity, and impaired rate performance[40]. Similar solvation dynamics are critical for other cations (e.g., Na^+, K^+, NH_4^+, and multivalent ions). For instance, density functional theory (DFT) simulations reveal that $[Mg(H_2O)_6]^{2+}$ exhibits a smaller hydration radius (2.1 Å vs. 2.2 Å of $[Zn(H_2O)_6]^{2+}$) and higher binding energy (−4.14 eV vs. −1.72 eV for Zn^{2+}), highlighting the role of cation-water interactions in low-temperature kinetics, as shown in Fig. 11**d** [156]. Modifying the coordination environment between cations and water—specifically by weakening their interaction strength—is a critical strategy for tailoring the solvation structure. This adjustment lowers the energy barrier for de-solvation of cations, thereby enhancing ion transport kinetics and improving electrochemical performance under low-temperature conditions.

Reconstructing the solvation structure by selecting appropriate zinc salts and increasing salt concentration has been shown to positively influence the electrochemical performance of zinc-based batteries. High-concentration electrolytes, in particular, offer notable advantages

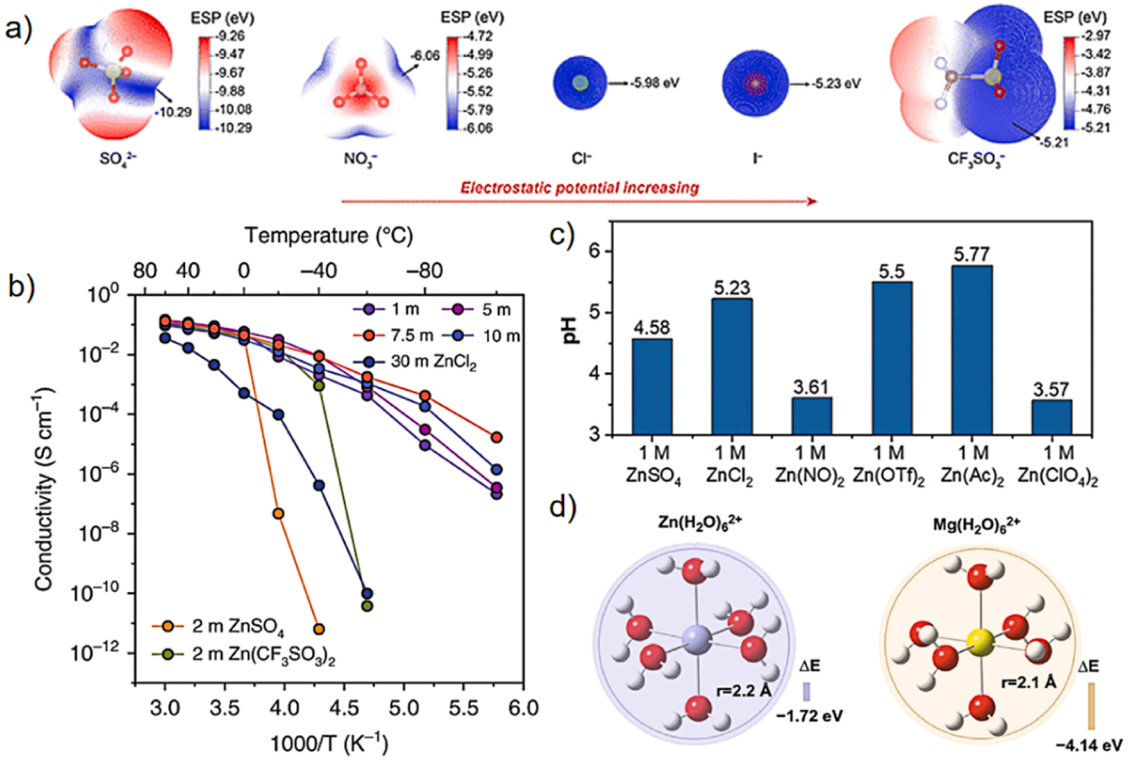

Fig. 11. Salt selection: a) ESP mapping of the selected anions [154]. b) Ionic conductivity of different electrolytes within the temperature range of −100 to 60 °C [40]. c) pH values of different zinc salts at the same concentration [155]. d) Formation energy and hydration radius of the solvation configuration of Zn^{2+} and the solvation configuration of Mg^{2+} were calculated [156].

such as enhanced ionic conductivity and improved low-temperature stability under low-temperature conditions. However, their practical implementation is often constrained by elevated viscosity, increased materials cost and processing complexity. Therefore, while high-concentration systems hold significant promise, further optimization is required to balance electrochemical performance with economic and operational feasibility, especially for scalable applications.

3.2.2. High entropy electrolyte

In conventional aqueous electrolytes, cation solvation is predominantly governed by water molecules, resulting in a high abundance of free water that adversely affects ionic conductivity at low temperatures. While increasing the salt concentration to create a high-concentration electrolyte can effectively depress the freezing point, this approach promotes the formation of extended anion-cation clusters that risk salt precipitation at subzero temperatures. In contrast, high-entropy electrolytes (HEEs) address these limitations through the strategic incorporation of supporting salts, which disrupt long-range ion aggregates and promote shorter, more mobile solvation structures. This structural modification significantly enhances low-temperature ion transport capabilities while maintaining solution stability.

For example, by introducing lithium bromide (LiBr) as a supporting salt into an aqueous $ZnBr_2$ electrolyte, a high-entropy electrolyte with the composition $Li_2ZnBr_4{\cdot}9H_2O$ was successfully formulated[170]. The bromide ions contributed by LiBr facilitate the tetrahedral coordination of Zn^{2+}, thus effectively suppressing the formation of extended $[ZnBr_{4\text{-}m}^{2\text{-}m}]_n$ ($n > 3$) networks, as illustrated in Fig. 12**a**. This configuration promotes the dissociation of LiBr and intensifies competition among Zn-Br aggregates, resulting in a predominance of short-chain species ($n \leq 3$). Consequently, the HB network of free water is disrupted, and water molecules are effectively excluded from the zinc solvation shell. Radial distribution function (RDF) analysis was employed to quantify the coordination numbers within the solvation structure of Zn^{2+}. In a 2 M $ZnBr_2$ electrolyte, Zn^{2+} exhibits a coordination number of 6 with water and nearly 0 with bromide (Fig. 12**c**), indicating a fully water-based solvation shell. As salt concentration increases, the Zn–H_2O coordination number decreases to 3.8, while Zn–Br coordination rises to 2.2 (Fig. 12d), signifying bromide incorporation into the solvation structure. Upon addition of LiBr, the Zn–H_2O coordination number further declines to 2, and Zn–Br coordination increases to 4 (Fig. 12**e**), confirming that high-entropy electrolytes facilitate water exclusion and anion integration. Meanwhile, Li^+ additionally binds free water molecules, further reducing the amount of free water in the electrolyte. Density functional theory (DFT) calculations were conducted to evaluate the LUMO energies of representative solvated structures across the three electrolytes. As shown in Fig. 12**b**, higher LUMO energy levels correlate with the improved reduction stability. The $[Zn(H_2O)_6]^{2+}$ in the 2 M $ZnBr_2$ electrolyte exhibits the lowest LUMO energy, whereas the $[ZnBr_4]^{2-}+4H_2O$ complex in $Li_2ZnBr_4{\cdot}9H_2O$ shows the highest, indicating enhanced electrochemical stability. These modifications yield exceptional low-temperature performance, with Zn// $NaV_3O_8{\cdot}1{\cdot}5H_2O$ batteries maintaining 71.2 % capacity retention after 800 cycles at –30 °C using the $Li_2ZnBr_4{\cdot}9H_2O$ electrolyte.

The high-entropy electrolyte (HEE) strategy represents a significant and innovative advancement in the development of aqueous zinc-ion batteries. Its principal strength lies in the rational design of a disordered solvation structure, which effectively addresses multiple long-standing challenges, including water activity, freezing point depression, salt precipitation, and zinc dendrite formation, within a unified framework. However, the practical implementation of this approach faces hurdles related to cost, scalability, and the handling of bromide-based chemistries. To enhance the commercial viability of HEEs, future research should investigate whether the underlying principles of entropy-driven solvation modulation can be extended to more abundant and cost-effective salt systems, such as chlorides or sulfates. Such efforts could pave the way for broader adoption of this promising strategy in large-scale energy storage applications.

3.2.3. Construction of solvation sheaths

Regulating the solvation structure of electrolytes is a pivotal strategy for ensuring their stable performance under low-temperature conditions. By introducing targeted additives or co-solvents, the coordination environment surrounding cations can be strategically modified, resulting in a reduced concentration of active water molecules. This structural modification inhibits ice nucleation and lowers the energy barrier for cation de-solvation, thereby significantly enhancing ion transport kinetics and electrochemical stability under low-temperature conditions.

Additives with polar functional groups play a central role in tailoring

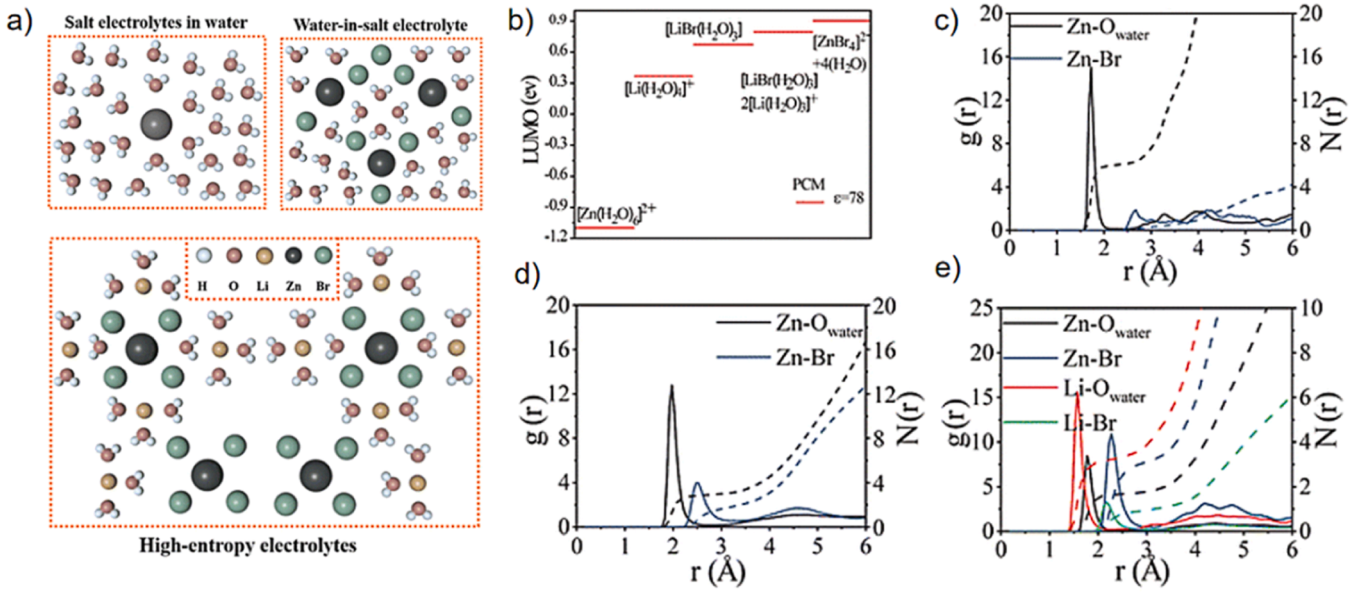

Fig 12. High-entropy systems: a) Schematic diagrams of solvation structures of salt-electrolytes in water, salt-in-water electrolytes, and high-entropy electrolytes [170]. b) Calculation of LUMO energy levels of different cation-water clusters using DFT [170].c) Radial distribution functions (RDFs) and coordination numbers (CNs) of Zn^{2+}-H_2O (O) and Zn^{2+}-Br in 2 m $ZnBr_2$ electrolyte [170]. (d) RDFs and CNs of Zn^{2+}-H_2O (O) and Zn^{2+}-Br in $ZnBr_2{\cdot}3H_2O$ electrolyte [170]. (e) RDFs and CNs of Zn^{2+}-H_2O (O), Zn^{2+}-Br, Li^+-H_2O (O) and Li-Br in the $Li_2ZnBr_4{\cdot}9H_2O$ electrolyte [170].

the solvation structure and are broadly categorized into hydrophilic and zinc-philic types in zinc-ion battery system[174]. Hydrophilic additives, such as those containing hydroxyl groups, form HBs with water molecules, disrupt the bulk H_2O network, and compete with Zn^{2+} for coordination, thereby reducing the number of water molecules in the Zn^{2+} solvation shell [175–176]. For instance, the incorporation of 40 vol % diethylene glycol monoethyl ether (DG) into a non-concentrated Zn $(OTf)_2$ aqueous electrolyte leads to the formation of a modified solvation sheath involving both DG and OTf^- anions (Fig. 13**f**)[171]. This structure disrupts the hydrogen-bond network, reduces free water content, and significantly lowers the electrolyte's freezing point. Moreover, DG promotes the formation of Zn^{2+}–OTf^- contact ion pairs (CIP), as evidenced by Fourier transform infrared (FTIR) spectra (Fig. 13**a**), where redshifts and peak enhancements at 1028 cm^{-1} (free OTf^-) and 1057 cm^{-1} (coordinated OTf^-) indicate strong interactions between OTf^-, DG, and Zn^{2+}. Similar vibrational trends in $–CF_3$ and $–SO_3$ groups (Fig. 13b) further confirm DG's role in regulating the coordination environment of OTf^- anions. Notably, at –35 °C, the DG40-based battery exhibits exceptional performance, achieving over 1000 cycles with ~99.9 % Coulombic efficiency and 99.8 % capacity retention at a current density of 2 A g^{-1} (Fig. 13**c**). Additionally, carbonyl-containing compounds, such as carboxylate salts and amides, possess a high donor density and are frequently employed as zinc-philic additives to coordinate with Zn^{2+} ions[175]. These additives can integrate into the primary solvation shell of Zn^{2+} by replacing water molecules or adsorb onto the anode surface, thereby modulating the de-solvation process of solvated Zn^{2+}. A representative system, ZN-1–3, is synthesized using $Zn(ClO_4)_2{\cdot}6H_2O$ and N-methylacetamide (NMA) in a 1:3 molar ratio [173]. In this electrolyte, Zn^{2+} forms complexes with NMA, H_2O, and ClO_4^-, resulting in a reduced hydration number compared to conventional aqueous electrolytes. This decrease in active water molecules effectively suppresses side reactions and expands the electrochemical stability window from approximately 2.4 V to 2.8 V. Molecular dynamics simulations (Fig. 13**h**) reveal that NMA replaces a water molecule in the primary solvation sheath, forming the $[Zn(ClO_4)_2(NMA)(H_2O)_3]$ complex. This structural transformation underpins the enhanced electrochemical performance of the ZN-1–3 electrolyte.

Beyond the above-mentioned compounds, other polar molecules have also been investigated as electrolyte additives to regulate the solvation structure. A notable example involves the incorporation of low-polarity 1,2-dimethoxyethane (DME) into a diluted 1 M $Zn(OTf)_2$ aqueous solution, resulting in a distinctive "core–shell" solvation sheath [172], as shown in Fig. 13***g*** This configuration features an OTf^--rich Zn^{2+} primary solvation sheath (PSS, core) surrounded by a DME-modulated outer sheath. Although DME does not directly participate in Zn^{2+}–PSS coordination, its presence enhances the Zn–OTf^- interaction, thereby optimizing the solvation structure for improved reaction kinetics at ultra-low temperatures. The resulting 1 M–$D_{0.15}$ electrolyte enables exceptional performance, achieving 3500 h of cycling stability at –40 °C and 3 mAh cm^{-2}, with a depth of discharge (DOD) of 51.3 % (Fig. 13**e**) [172]. Furthermore, in Zn||Cu cells, the Coulombic efficiency remains stable at 99.1 % under –40 °C, and after 500 cycles, the voltage polarization is maintained at approximately 325 mV at 0.2 mA cm^{-2} (Fig. 13**d**)[172].

Overall, electrolyte additives serve as powerful tools for solvation regulation in high-performance zinc-based batteries. The incorporation of hydrophilic and zinc-philic compounds not only reduces the number of solvated water molecules around Zn^{2+} but also suppresses parasitic reactions and modifies the solid–electrolyte interphase (SEI). These changes influence the deposition morphology, nucleation behavior, and

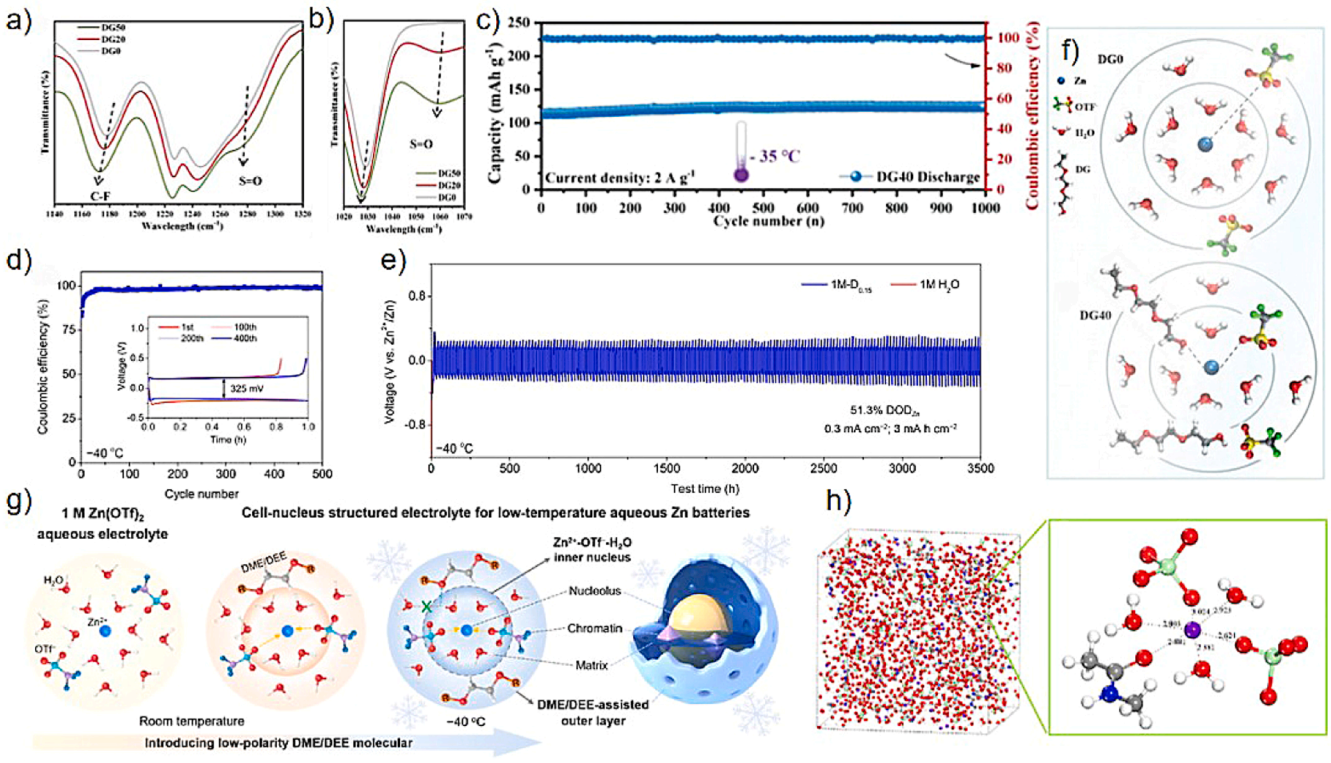

Fig. 13. Construction of solvation sheaths with additives: The Raman spectrum of the electrolyte is between (a)1140 and 1320 cm^{-1} [171]. b) Between 1020 and 1070 cm^{-1} [171]. C) Cycling stability of Zn//PANI coin cells under 2 A g^{-1} at –35 °C [171]. d) Zn plating/stripping CE and voltage curves (inset) of Zn|1M-$D_{0.15}$|Cu half-cell at –40 °C (0.2 mA cm^{-2} and 0.2 mA h cm^{-2}) [172]. e) Cycling performance of Zn//Zn cells (0.3 mA cm^{-2} and 3 mA h cm^{-2}) at –40 °C [172]. f) Schematic diagram of the solvation structure of Zn^{2+} in hybrid electrolyte and DG40 electrolyte [171]. g) Schematic diagram of the electrolyte design for the nuclear structure of low-temperature water-zinc batteries [172]. h) The three-dimensional snapshot obtained by MD simulation and the solvation structure of Zn^{2+}in the ZN-1–3 electrolyte [173].

electron transfer kinetics, collectively contributing to enhanced battery performance under extreme conditions.

3.2.4. Regulation of solvent environment

While aqueous electrolytes are essential for enabling ion transport and electrochemical reactions in zinc-ion batteries (ZIBs), the high reactivity of solvent molecules—particularly water—can compromise the stability of electrode-electrolyte interfaces, ultimately leading to parasitic reactions and degradation of battery performance[177,178]. A central challenge, therefore, lies in optimizing the solvent environment to support both fast ion transport and stable interfacial electrochemical processes. Solvent environment regulation involves tailoring the spatial arrangement and interactions of solvent molecules within the electrolyte to modulate the solvation structure around Zn^{2+} ions. This can be achieved through the strategic introduction of non-polar solvents, amphiphilic salts, or co-solvents that reshape the coordination landscape and suppress undesirable water activity.

A notable example is the development of a surface-free microemulsion electrolyte (SFMEE) based on a water-in-oil Möbius polar topology, as illustrated in Fig. 14**a**[179]. This system integrates oil, water and amphiphilic salts to form a unique solvation structure. The blank electrolyte (BE) consists of a 1 M $Zn(OTf)_2$ aqueous solution, while the high-concentration electrolyte (HCE) is 3 M $Zn(OTf)_2$ in H_2O. In this system, the non-polar solvent CPME (–C–O–C–) engages in HBs with H_2O (–OH), initially orienting the polar head inward. As the interaction dynamics evolve, OTf^- acts as a molecular bridge to link CPME and H_2O: its $–SO_3$ group forms HBs with H_2O, while its $–CF_3$ group engages with the non-polar CPME region[180]. This dual interaction induces a polarity inversion, reorienting the CPME polar head outward and ultimately facilitating the formation of a Möbius polarity topological solvation structure. A variety of spectral techniques have confirmed the unique solvation structure and its evolution of SFMEE. Spectroscopic analyses confirm the unique solvation behavior of SFMEE. Infrared spectra of C–F and $S=O$ (Fig. 14**c**) reveal distinct vibrational patterns for free and coordinated OTf^-, with redshifts and peak splitting observed in both HCE and SFMEE, indicating OTf^- participation in solvation across inner and outer sheaths[181]. Nuclear magnetic resonance (NMR) further elucidates these interactions: in HCE, OTf^- coordination increases the electron cloud density around ^{19}F, causing a high-field shift (Fig. 14**d**), a trend also observed in SFMEE. For ^1H, BE shows a high-field shift due to water's solvation role; in HCE, reduced free water and increased solvation lead to further high-field shifts. In contrast, SFMEE's water-in-oil structure confines inner solvated H_2O within an outer CPME layer, restricting HB expansion and decreasing ^1H electron cloud density, resulting in a low-field shift (Fig. 14**e**). The Möbius solvation structure enables encapsulation of water molecules within the inner layer of the non-polar CPME solvent, while the outer layer remains non-polar. Activation energy for de-solvation was determined using the Arrhenius equation, revealing that the bilayer configuration does not impede de-solvation. In fact, its activation energy (25.34 kJ mol^{-1}) is lower than that of BE and HCE, attributed to the direct interaction between solvated molecules and Zn^{2+} ions[182]. The Zn||NVO battery demonstrates excellent low-temperature performance, maintaining 86.5 % capacity retention over 1000 cycles at −30 °C (Fig. 14***g***). To assess the universality of the SFMEE system, five hydrophobic solvents—methyl ethyl carbonate ($C_4H_8O_3$), diethyl adipate ($C_{10}H_{18}O_4$), benzyl alcohol (C_7H_8O), n-butyl acetate ($C_6H_{12}O_2$), and diethyl carbonate ($C_5H_{10}O_3$)—were evaluated for their ability to form Möbius-type solvation structures. The Zn||Zn cells assembled with these solvents exhibited consistently high performance, confirming the broad applicability of SFMEE in ZIBs (Fig. 14**f**).

In summary, the construction of a non-polar solvent environment and the regulation of topological solvation structures—such as the oil-in-water Möbius configuration—offer a powerful strategy for stabilizing electrode interfaces and enhancing low-temperature performance in aqueous ZIBs (Fig. 14**b**). This dual regulation of solvent polarity and solvation architecture represents a promising direction for future electrolyte design.

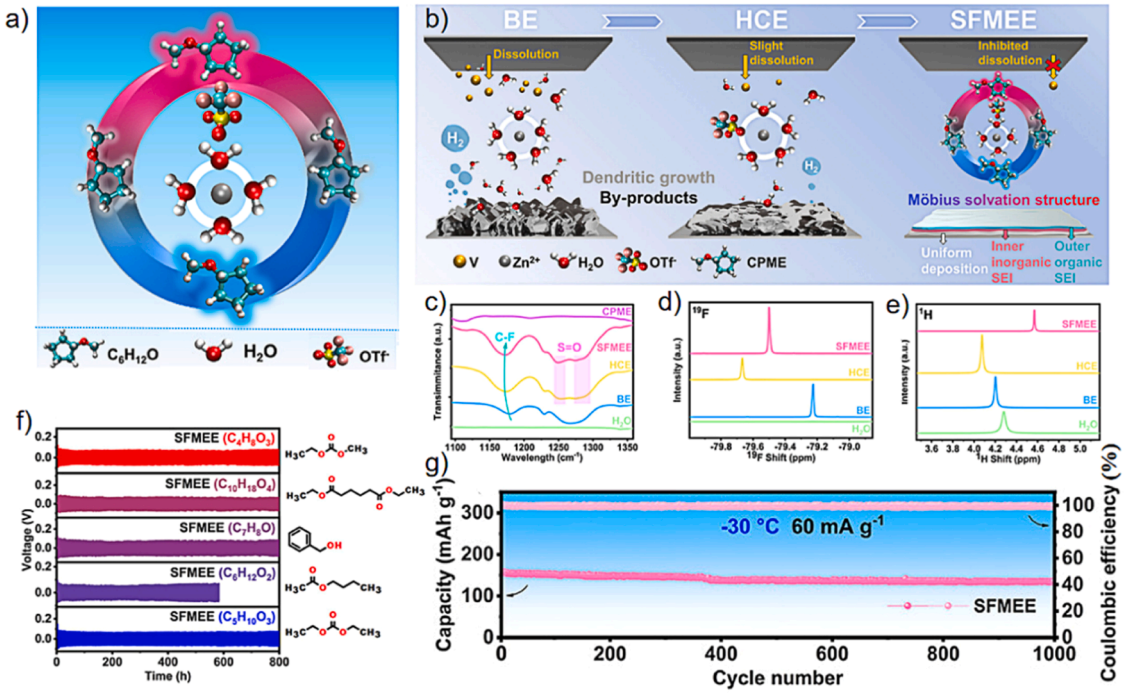

Fig. 14. Solvent environment regulation: a) Schematic diagram of the polar topological solvation structure of the water-in-oil type Mobius [179]. b) Schematic diagram of the action mechanism of different electrolytes [179]. c) Infrared spectra of different electrolytes. d) [19]F NMR spectra of different electrolytes [179]. e) ^1H NMR spectra of different electrolytes [179]. f) Performance of Zn//Zn and Zn//NVO batteries at –30 °C [179]. g) Performance of Zn// zinc batteries at 1 mA cm^{-2} and different SFMEE [179].

4. Conclusion and prospect

Understanding the intrinsic physicochemical properties of aqueous electrolytes is fundamental to advancing their performance under low-temperature conditions. This review elucidates the thermodynamic and kinetic alterations in HB networks and solvation structures induced by low temperatures, providing a foundation for electrolyte optimization strategies. Current research efforts predominantly focus on modulating HB interactions and tailoring solvation architectures to suppress water crystallization and enhance ion transport. The freezing of water is widely recognized as a phase transition from a disordered liquid to an ordered ice lattice, driven by HB formation. Therefore, lowering the freezing point of aqueous electrolytes fundamentally requires disruption of the native HB network. Various solvation structures have been shown to improve low-temperature battery performance to varying extents. Key strategies include the development of high-concentration electrolytes, eutectic systems, functional additives and co-solvents, structural modulation of electrolytes, high-entropy formulations, and solvent environment engineering. For instance, ions with high charge density and small ionic radii exhibit strong interactions with water molecules, which thermodynamically favor a reduction in enthalpy (ΔH), thereby contributing to improved low-temperature electrolyte behavior. Additives and co-solvents can modulate the HB network by disrupting, reorganizing, or reinforcing HB interactions. Additionally, altering the solvation structure through molecular design is a widely adopted approach to suppress freezing and enhance electrochemical stability. Collectively, these methods address both thermodynamic (e.g., freezing point depression) and kinetic (e.g., ion transport) challenges, offering a multifaceted pathway to optimize the performance of electrolytes under low-temperature conditions.

Despite significant progress, the full potential of electrolyte engineering for low-temperature aqueous batteries remains unrealized. Several critical challenges must be addressed to bridge the gap between laboratory innovation and commercial application:

I. **Elucidating Fundamental Mechanisms**: A deeper mechanistic understanding is paramount. Advanced theoretical calculations, particularly MD simulations and DFT, are essential to decode the complex interplay between ion coordination, hydrogen bond (HB) network dynamics, viscosity, and transport kinetics. This is especially crucial at ultra-low temperatures, where classical models like the Arrhenius equation often break down. MD and DFT can provide molecular- and atomic-level insights into HB length, angle, and coordination patterns in both liquid and solid states, guiding the rational design of electrolytes.

II. **Probing Dynamic Processes with Advanced Characterization**: Moving beyond static analysis, the integration of in-situ and operando characterization techniques (e.g., Raman, NMR, synchrotron X-ray) is vital to dynamically track the evolution of solvation structures and HB networks during battery operation. Coupling these rich datasets with machine learning for high-throughput analysis will enable the predictive design of electrolytes and unravel complex structure-property relationships.

III. **Developing Hybrid Electrolyte Systems**: Future efforts must move beyond single-approach solutions. The next frontier lies in designing hybridized electrolytes that synergistically combine moderate-concentration salts, low-freezing-point co-solvents, and functional additives. This integrated strategy can simultaneously tackle the interconnected challenges of freezing suppression, ionic conductivity enhancement, and interfacial stability, holistically addressing both the thermodynamic and kinetic hurdles of low-temperature operation.

IV. **Ensuring Sustainability and Commercial Viability**: To ensure commercial viability for large-scale energy storage, performance cannot be the sole metric. Research must prioritize the development of high-performance electrolytes based on earth-abundant, non-toxic, and low-cost components. Overcoming the cost and environmental scalability of advanced electrolyte formulations is an essential step toward translating promising laboratory breakthroughs into commercially viable, sustainable low-temperature aqueous batteries.

Overcoming these challenges will be pivotal in transitioning low-temperature aqueous electrolytes from laboratory innovations to commercially viable solutions for energy storage in cold climates and extreme environments. Continued interdisciplinary efforts—spanning materials science, electrochemistry, computational modeling, and data-driven design—will be key to realizing this vision.

CRediT authorship contribution statement

Liwen Pan: Writing – original draft, Writing – review & editing. **Nannan Jia:** Investigation, Writing – original draft, Writing – review & editing. **Jie Yang:** Conceptualization, Supervision, Writing – original draft, Writing – review & editing. **Xinhua Liu:** Conceptualization, Supervision. **Rui Tan:** Conceptualization, Supervision, Writing – original draft, Writing – review & editing.

Declaration of competing interest

The authors declare that they have no known competing financial interests or personal relationships that could have appeared to influence the work reported in this paper.

Data availability

Data will be made available on request.

References

[1] A. Eldering, P. Wennberg, D. Crisp, D. Schimel, M. Gunson, A. Chatterjee, J. Liu, F. Schwandner, Y. Sun, C. O'dell, The Orbiting Carbon Observatory-2 early science investigations of regional carbon dioxide fluxes, Science (1979) 358 (6360) (2017) eaam5745, https://doi.org/10.1126/science.aam5745.
[2] N. Liu, Y. Zhan, R. Tan, G. Zhao, J. Song, Unlocking carbon capture and storage potential: policy incentives, economic challenges, and infrastructure integration for CO_2 transport, Chain 2 (3) (2025) 211–226, https://doi.org/10.23919/chain.2025.000015.
[3] W. Chen, Y. Hu, Y. Liu, S. Wang, A. Hu, T. Lei, Y. Li, P. Li, D. Chen, L. Xia, Ultralong cycling and safe lithium–sulfur pouch cells for sustainable energy storage, Adv. Mater. 36 (21) (2024) 2312880, https://doi.org/10.1002/adma.202312880.
[4] C.-H. Wu, K.-C. Wu, C.-H. Shen, C.-W. Kung, Zirconium-based metal–organic frameworks for electrochemical energy storage, Coord. Chem. Rev. 538 (2025) 216704, https://doi.org/10.1016/j.ccr.2025.216704.
[5] H. Li, B. Huang, M. Chuai, Z. Zheng, H. Chen, Z. Piao, G. Zhou, H.J. Fan, Dual-plating aqueous Zn–iodine batteries enabled via halogen-complexation chemistry for large-scale energy storage, Energy Environ. Sci. 18 (7) (2025) 3160–3168, https://doi.org/10.1039/d5ee00027k.
[6] Z. Zhu, T. Jiang, M. Ali, Y. Meng, Y. Jin, Y. Cui, W. Chen, Rechargeable batteries for grid scale energy storage, Chem. Rev. 122 (22) (2022) 16610–16751, https://doi.org/10.1021/acs.chemrev.2c00289.
[7] Z. Jia, H. Shen, J. Kou, T. Zhang, Z. Wang, W. Tang, M. Doeff, C.Y. Chiang, K. Chen, Solid electrolyte bimodal grain structures for improved cycling performance, Adv. Mater. 36 (18) (2024) 2309019, https://doi.org/10.1002/adma.202309019.
[8] S. Yuan, X. Huang, T. Kong, L. Yan, Y. Wang, Organic electrode materials for energy storage and conversion: mechanism, characteristics, and applications, Acc. Chem. Res. 57 (10) (2024) 1550–1563, https://doi.org/10.1021/acs.accounts.4c00016.
[9] J. Li, P. Ruan, X. Chen, S. Lei, B. Lu, Z. Chen, J. Zhou, Aqueous batteries for human body electronic devices: focus Review, ACS. Energy Lett. 8 (7) (2023) 2904–2918, https://doi.org/10.1021/acsenergylett.3c00678.
[10] S. Deng, B. Xu, J. Zhao, H. Fu, Advanced design for anti-freezing aqueous zinc-ion batteries, Energy Storage Mater. 70 (2024) 103490, https://doi.org/10.1016/j.ensm.2024.103490.
[11] M. Han, T.C. Li, X. Chen, H.Y. Yang, Electrolyte modulation strategies for low-temperature Zn batteries, Small. 20 (3) (2024) 2304901, https://doi.org/10.1002/smll.202304901.
[12] M. Li, X. Wang, J. Hu, J. Zhu, C. Niu, H. Zhang, C. Li, B. Wu, C. Han, L. Mai, Comprehensive H_2O molecules regulation via deep eutectic solvents for ultra-

stable zinc metal anode, Angew. Chem. 135 (8) (2023) e202215552, https://doi.org/10.1002/ange.202215552.
[13] F.H. Hashim, F. Yu, E.I. Izgorodina, Appropriate clusterset selection for the prediction of thermodynamic properties of liquid water with QCE theory, Phys. Chem. Chem. Phys. 25 (14) (2023) 9846–9858, https://doi.org/10.1039/d2cp03712b.
[14] H. Elgabarty, T.D. Kühne, Tumbling with a limp: local asymmetry in water's hydrogen bond network and its consequences, Phys. Chem. Chem. Phys. 22 (19) (2020) 10397–10411, https://doi.org/10.1039/c9cp06960g.
[15] S. Chen, M. Zhang, P. Zou, B. Sun, S. Tao, Historical development and novel concepts on electrolytes for aqueous rechargeable batteries, Energy Environ. Sci. 15 (5) (2022) 1805–1839, https://doi.org/10.1039/d2ee00004k.
[16] A. Naveed, T. Rasheed, B. Raza, J. Chen, J. Yang, N. Yanna, J. Wang, Addressing thermodynamic Instability of Zn anode: classical and recent advancements, Energy Storage Mater. 44 (2022) 206–230, https://doi.org/10.1016/j.ensm.2021.10.005.
[17] D. Hubble, D.E. Brown, Y. Zhao, C. Fang, J. Lau, B.D. McCloskey, G. Liu, Liquid electrolyte development for low-temperature lithium-ion batteries, Energy Environ. Sci. 15 (2) (2022) 550–578, https://doi.org/10.1039/d1ee01789f.
[18] H. Jia, X. Jiang, Y. Wang, Y. Lam, S. Shi, G. Liu, Hybrid co-solvent-induced high-entropy electrolyte: regulating of hydrated Zn^{2+} solvation structures for excellent reversibility and wide temperature adaptability, Adv. Energy Mater. 14 (18) (2024) 2304285, https://doi.org/10.1002/aenm.202304285.
[19] C. Li, R. Kingsbury, L. Zhou, A. Shyamsunder, K.A. Persson, L.F. Nazar, Tuning the solvation structure in aqueous zinc batteries to maximize Zn-ion intercalation and optimize dendrite-free zinc plating, ACS. Energy Lett. 7 (1) (2022) 533–540, https://doi.org/10.1021/acsenergylett.1c02514.
[20] X.-X. Zhang, Y.-Q. Chen, C.-X. Lin, Y.-S. Lin, G.-L. Hu, Y.-C. Liu, X.-L. Xue, S.-J. Chen, Z.-L. Yang, B.-S. Sa, Y.-N. Zhang, Restraining growth of Zn dendrites by poly dimethyl diallyl ammonium cations in aqueous electrolytes, Rare Metals. 43 (8) (2024) 3735–3747, https://doi.org/10.1007/s12598-023-02561-0.
[21] B.-R. Xu, Q.-A. Li, Y. Liu, G.-B. Wang, Z.-H. Zhang, F.-Z. Ren, Urea-induced interfacial engineering enabling highly reversible aqueous zinc-ion battery, Rare Metals. 43 (4) (2024) 1599–1609, https://doi.org/10.1007/s12598-023-02541-4.
[22] X.-M. Yan, H. Li, B.-L. Zhang, B.-H. Chen, W. Xiao, Constructing a high-performance cathode for aqueous zinc ion batteries via understanding the energy storage mechanism of MnO, Rare Metals. 44 (1) (2024) 218–229, https://doi.org/10.1007/s12598-024-02938-9.
[23] L.-K. Zhao, X.-W. Gao, T.-Z. Ren, D. Wang, D.-W. Wang, Z.-M. Liu, H. Chen, W.-B. Luo, Regulating ion transport behaviors toward dendrite-free potassium metal batteries: recent advances and perspectives, Rare Metals. 43 (4) (2024) 1435–1460, https://doi.org/10.1007/s12598-023-02537-0.
[24] W.-W. Wang, R. Huang, Y. Tao, P. He, S.-X. Tuo, Y.-J. Bian, R.-T. Hu, J. Yan, Y.-J. Liang, W.-C. Zhang, Construction of a multifunctional $Ti_3C_2T_x$ MXene/g-C_3N_4 artificial protective layer for dendrite-free aqueous Zn-ion batteries, Rare Metals. 43 (10) (2024) 4992–5004, https://doi.org/10.1007/s12598-024-02739-0.
[25] H.-X. Wu, K.-L. Guo, Nuclei-rich galvanizing strategy for suppressing zinc dendrite growth, Rare Metals. 43 (8) (2024) 4016–4018, https://doi.org/10.1007/s12598-024-02745-2.
[26] Y.-D. Ma, H.-N. Zhu, Y. Le, Y.-H. Liu, T.-H. Mei, S.-J. Bao, M.-W. Xu, Construction of sodium-poor and oxygen defect-rich vanadium oxide nanobelts for high-performance aqueous zinc-ion batteries, Rare Metals. 44 (1) (2024) 230–239, https://doi.org/10.1007/s12598-024-02940-1.
[27] Z. Li, Y.X. Yao, S. Sun, C.B. Jin, N. Yao, C. Yan, Q. Zhang, 40 Years of Low-Temperature Electrolytes for Rechargeable Lithium Batteries, Angew. Chem. 135 (37) (2023) e202303888, https://doi.org/10.1002/ange.202303888.
[28] L. Jiang, D. Dong, Y.-C. Lu, Design strategies for low temperature aqueous electrolytes, Nano Res. Energy 1 (1) (2022) e9120003, https://doi.org/10.26599/nre.2022.9120003.
[29] K.H. Kim, K. Amann-Winkel, N. Giovambattista, A. Späh, F. Perakis, H. Pathak, M. L. Parada, C. Yang, D. Mariedahl, T. Eklund, T.J. Lane, S. You, S. Jeong, M. Weston, J.H. Lee, I. Eom, M. Kim, J. Park, S.H. Chun, P.H. Poole, A. Nilsson, Experimental observation of the liquid-liquid transition in bulk supercooled water under pressure, Science (1979) 370 (6519) (2020) 978, https://doi.org/10.1126/science.abb9385.
[30] C. Huang, K.T. Wikfeldt, T. Tokushima, D. Nordlund, Y. Harada, U. Bergmann, M. Niebuhr, T.M. Weiss, Y. Horikawa, M. Leetmaa, M.P. Ljungberg, O. Takahashi, A. Lenz, L. Ojamäe, A.P. Lyubartsev, S. Shin, L.G.M. Pettersson, A. Nilsson, The inhomogeneous structure of water at ambient conditions, Proc. Natl. Acad. Sci. USA 106 (36) (2009) 15214–15218, https://doi.org/10.1073/pnas.0904743106.
[31] M. Matsumoto, S. Saito, I. Ohmine, Molecular dynamics simulation of the ice nucleation and growth process leading to water freezing, Nature 416 (6879) (2002) 409–413, https://doi.org/10.1038/416409a.
[32] I. Alkorta, I. Rozas, J. Elguero, Non-conventional hydrogen bonds, Chem. Soc. Rev. 27 (2) (1998) 163–170, https://doi.org/10.1039/a827163z.
[33] Y. Chen, H.I. Okur, N. Gomopoulos, C. Macias-Romero, P.S. Cremer, P. B. Petersen, G. Tocci, D.M. Wilkins, C. Liang, M. Ceriotti, Electrolytes induce long-range orientational order and free energy changes in the H-bond network of bulk water, Sci. Adv. 2 (4) (2016) e1501891, https://doi.org/10.1126/sciadv.1501891.
[34] T. Steiner, The hydrogen bond in the solid state, Angew. Chem. Int. Ed. 41 (1) (2002) 48–76, https://doi.org/10.1002/1521-3773(20020104)41:1<48::AID−NIE48>3.0.CO;2-U.
[35] P.A. Hunt, C.R. Ashworth, R.P. Matthews, Hydrogen bonding in ionic liquids, Chem. Soc. Rev. 44 (5) (2015) 1257–1288, https://doi.org/10.1039/c4cs00278d.
[36] P.A. Kollman, L. Allen, Theory of the hydrogen bond, Chem. Rev. 72 (3) (1972) 283–303, https://doi.org/10.1021/cr60277a004.
[37] C.Q. Sun, X. Zhang, X. Fu, W. Zheng, J.-l. Kuo, Y. Zhou, Z. Shen, J. Zhou, Density and phonon-stiffness anomalies of water and ice in the full temperature range, J. Phys. Chem. Lett. 4 (19) (2013) 3238–3244, https://doi.org/10.1021/jz401380p.
[38] L. Ma, S. Chen, N. Li, Z. Liu, Z. Tang, J.A. Zapien, S. Chen, J. Fan, C. Zhi, Hydrogen-free and dendrite-free all-solid-state Zn-ion batteries, Adv. Mater. 32 (14) (2020) 1908121, https://doi.org/10.1002/adma.201908121.
[39] S. Emamian, T. Lu, H. Kruse, H. Emamian, Exploring nature and predicting strength of hydrogen bonds: a correlation analysis between atoms-in-molecules descriptors, binding energies, and energy components of symmetry-adapted perturbation theory, J. Comput. Chem. 40 (32) (2019) 2868–2881, https://doi.org/10.1002/jcc.26068s.
[40] Q. Zhang, Y. Ma, Y. Lu, L. Li, F. Wan, K. Zhang, J. Chen, Modulating electrolyte structure for ultralow temperature aqueous zinc batteries, Nat. Commun. 11 (1) (2020) 4463, https://doi.org/10.1038/s41467-020-18284-0.
[41] A. Luzar & D.J.N. Chandler. Hydrogen-bond kinetics in liquid water. 379(6560) (1996) 55–57.10.1038/379055a0.
[42] A. Chakrabortty, S. Bandyopadhyay, Probing the degree of restriction in solvent dynamics at the interface of a protein–RNA complex, J. Phys. Chem. B 129 (17) (2025) 4143–4158, https://doi.org/10.1021/acs.jpcb.4c08804.
[43] A.R. Bizzarri, S.J. Cannistraro, Molecular dynamics of water at the protein−solvent interface, J. Phys. Chem. B 106 (26) (2002) 6617–6633, https://doi.org/10.1021/jp020100m.
[44] F.H. Stillinger, Theory and molecular models for water, Adv. Chem. Phys. (1975) 1–101, https://doi.org/10.1002/9780470143834.
[45] D. Rapaport, Hydrogen bonds in water: network organization and lifetimes, Mol. Phys. 50 (5) (1983) 1151–1162, https://doi.org/10.1080/00268978300102931.
[46] S. Paul, A. Chandra, Hydrogen bond dynamics at vapour–water and metal–water interfaces, Chem. Phys. Lett. 386 (4–6) (2004) 218–224, https://doi.org/10.1016/j.cplett.2003.12.120.
[47] A. Luzar, D. Chandler, Effect of environment on hydrogen bond dynamics in liquid water, Phys. Rev. Lett. 76 (6) (1996) 928–931, https://doi.org/10.1103/physrevlett.76.928.
[48] H. Xu, H.A. Stern, B. Berne, Can water polarizability be ignored in hydrogen bond kinetics? J. Phys. Chem. B 106 (8) (2002) 2054–2060, https://doi.org/10.1021/jp013426o.
[49] S. Bandyopadhyay, S. Chakraborty, B. Bagchi, Secondary structure sensitivity of hydrogen bond lifetime dynamics in the protein hydration layer, J. Am. Chem. Soc. 127 (47) (2005) 16660–16667, https://doi.org/10.1021/ja054462u.
[50] S. Genieva, L. Vlaev, A. Atanassov, Study of the thermooxidative degradation kinetics of poly (tetrafluoroethene) using iso-conversional calculation procedure, J. Therm. Anal. Calorim. 99 (2) (2010) 551–561, https://doi.org/10.1007/s10973-009-0191-4.
[51] Q. Li, Y. Li, M. Liu, Y. Li, H. Zhao, H. Ren, Y. Zhao, Q. Zhou, X. Feng, J. Shi, Elucidating thermal decomposition kinetic mechanism of charged layered oxide cathode for sodium-ion batteries, Adv. Mater. (2025) 2415610, https://doi.org/10.1002/adma.202415610.
[52] F.W. Starr, J.K. Nielsen, H.E. Stanley, Fast and slow dynamics of hydrogen bonds in liquid water, Phys. Rev. Lett. 82 (11) (1999) 2294, https://doi.org/10.1103/PhysRevLett.82.2294.
[53] E. Logan, E.M. Tonita, K. Gering, J. Li, X. Ma, L. Beaulieu, J. Dahn, A study of the physical properties of Li-ion battery electrolytes containing esters, J. Electrochem. Soc. 165 (2) (2018) A21, https://doi.org/10.1149/2.0271802jes.
[54] J.-P. Jones, S.C. Jones, F.C. Krause, J. Pasalic, M.C. Smart, R.V. Bugga, E. J. Brandon, W.C. West, Additive effects on Li‖ CF_x and Li‖ CF_x-MnO_2 primary cells at low temperature, J. Electrochem. Soc. 164 (13) (2017) A3109–A3116, https://doi.org/10.1149/2.0831713jes.
[55] Z. Huang, Z. Xiao, R. Jin, Z. Li, C. Shu, R. Shi, X. Wang, Z. Tang, W. Tang, Y. Wu, A comprehensive review on liquid electrolyte design for low-temperature lithium/sodium metal batteries, Energy Environ. Sci. 17 (15) (2024) 5365–5386, https://doi.org/10.1039/d4ee02060j.
[56] J. Han, A. Mariani, S. Passerini, A. Varzi, A perspective on the role of anions in highly concentrated aqueous electrolytes, Energy Environ. Sci. 16 (4) (2023) 1480–1501, https://doi.org/10.1039/d2ee03682g.
[57] M. Qiu, P. Sun, K. Han, Z. Pang, J. Du, J. Li, J. Chen, Z.L. Wang, W. Mai, Tailoring water structure with high-tetrahedral-entropy for antifreezing electrolytes and energy storage at− 80° C, Nat. Commun. 14 (1) (2023) 601, https://doi.org/10.1038/s41467-023-36198-5.
[58] M. Qiu, Y. Liang, J. Hong, J. Li, P. Sun, W. Mai, Entropy-driven hydrated eutectic electrolytes with diverse solvation configurations for all-temperature Zn-ion batteries, Angew. Chem. Int. Ed. 63 (38) (2024) e202407012, https://doi.org/10.1002/anie.202407012.
[59] B. Xie, C. Zheng, H. Lang, M. Li, Q. Hu, X. Tan, Q. Zheng, Y. Huo, J. Zhao, J.-L. Yang, Ultrastable electrolyte (>3500 h at high current density) achieved by high-entropy solvation toward practical aqueous zinc metal batteries, Energy Environ. Sci. 17 (19) (2024) 7281–7293, https://doi.org/10.1039/d4ee02896a.
[60] A. Ramanujapuram, G. Yushin, Understanding the exceptional performance of lithium-ion battery cathodes in aqueous electrolytes at subzero temperatures, Adv. Energy Mater. 8 (35) (2018) 1802624, https://doi.org/10.1002/aenm.201802624.
[61] Y. Zhao, Z. Chen, F. Mo, D. Wang, Y. Guo, Z. Liu, X. Li, Q. Li, G. Liang, C. Zhi, Aqueous rechargeable metal-ion batteries working at subzero temperatures, Adv. Sci. 8 (1) (2021) 2002590, https://doi.org/10.1002/advs.202002590.

[62] Y. Wang, H. Wei, Z. Li, X. Zhang, Z. Wei, K. Sun, H.J.T.C.R. Li, Optimization strategies of electrolytes for low-temperature aqueous batteries, Chem. Record 22 (10) (2022) e202200132, https://doi.org/10.1002/tcr.202200132.
[63] J. Tan, J. Liu, Electrolyte engineering toward high-voltage aqueous energy storage devices, Energy Environ. Mater. 4 (3) (2021) 302–306, https://doi.org/10.1002/eem2.12125.
[64] M.S. Ding, K. Xu, Phase diagram, conductivity, and glass transition of LiTFSI–H_2O binary electrolytes, J. Phys. Chem. C 122 (29) (2018) 16624–16629, https://doi.org/10.1021/acs.jpcc.8b05193.
[65] L. Jiang, S. Han, Y.-C. Hu, Y. Yang, Y. Lu, Y.-C. Lu, J. Zhao, L. Chen, Y.-S. Hu, Rational design of anti-freezing electrolytes for extremely low-temperature aqueous batteries, Nat. Energy 9 (7) (2024) 839–848, https://doi.org/10.1038/s41560-024-01527-5.
[66] Y. Zhang, P.S. Cremer, Chemistry of Hofmeister anions and osmolytes, Annu. Rev. Phys. Chem. 61 (1) (2010) 63–83, https://doi.org/10.1146/annurev.physchem.59.032607.093635.
[67] Y. Marcus, Effect of ions on the structure of water: structure making and breaking, Chem. Rev. 109 (3) (2009) 1346–1370, https://doi.org/10.1021/cr8003828.
[68] K.D. Collins, Ions from the Hofmeister series and osmolytes: effects on proteins in solution and in the crystallization process, Methods 34 (3) (2004) 300–311, https://doi.org/10.1016/j.ymeth.2004.03.021.
[69] S.C. Flores, J. Kherb, N. Konelick, X. Chen, P.S. Cremer, The effects of Hofmeister cations at negatively charged hydrophilic surfaces, J. Phys. Chem. C 116 (9) (2012) 5730–5734, https://doi.org/10.1021/jp210791j.
[70] I. Popov, Z. Zhu, A.R. Young-Gonzales, R.L. Sacci, E. Mamontov, C. Gainaru, S. J. Paddison, A.P. Sokolov, Search for a Grotthuss mechanism through the observation of proton transfer, Commun. Chem. 6 (1) (2023) 77, https://doi.org/10.1038/s42004-023-00878-6.
[71] T. Miyake, M. Rolandi, Grotthuss mechanisms: from proton transport in proton wires to bioprotonic devices, J. Phys. 28 (2) (2015) 023001, https://doi.org/10.1088/0953-8984/28/2/023001.
[72] Y. Lu, W. Zhang, S. Liu, Q. Cao, S. Yan, H. Liu, W. Hou, P. Zhou, X. Song, Y. Ou, Tuning the Li^+ solvation structure by a "bulky coordinating" strategy enables nonflammable electrolyte for ultrahigh voltage lithium metal batteries, ACS. Nano 17 (10) (2023) 9586–9599, https://doi.org/10.1021/acsnano.3c02948.
[73] L. Li, H. Cheng, J. Zhang, Y. Guo, C. Sun, M. Zhou, Q. Li, Z. Ma, J. Ming, Quantitative chemistry in electrolyte solvation design for aqueous batteries, ACS. Energy Lett. 8 (2) (2023) 1076–1095, https://doi.org/10.1021/acsenergylett.2c02585.
[74] Y.-S. Hu & H.J.A.E.L. Pan. Solvation structures in electrolyte and the interfacial chemistry for Na-ion batteries. 7(12)(2022) 4501–4503.10.1021/acsenergylett.2c02529.
[75] J. Hao, X. Li, X. Zeng, D. Li, J. Mao, Z. Guo, Deeply understanding the Zn anode behaviour and corresponding improvement strategies in different aqueous Zn-based batteries, Energy Environ. Sci. 13 (11) (2020) 3917–3949, https://doi.org/10.1039/d0ee02162h.
[76] J. Cao, D. Zhang, X. Zhang, Z. Zeng, J. Qin, Y. Huang, Strategies of regulating Zn^{2+} solvation structures for dendrite-free and side reaction-suppressed zinc-ion batteries, Energy Environ. Sci. 15 (2) (2022) 499–528, https://doi.org/10.1039/d1ee03377h.
[77] M. Hartmann, T. Clark, R. van Eldik, Hydration and water exchange of zinc (II) ions. Application of density functional theory, J. Am. Chem. Soc. 119 (33) (1997) 7843–7850, https://doi.org/10.1021/ja970483f.
[78] S. Lee, J. Kim, J.K. Park, K.S. Kim, Ab initio study of the structures, energetics, and spectra of Aquazinc (II), J. Phys. Chem. 100 (34) (1996) 14329–14338, https://doi.org/10.1021/jp960714p.
[79] Z. Tian, Y. Zou, G. Liu, Y. Wang, J. Yin, J. Ming, H.N. Alshareef, Electrolyte solvation structure design for sodium ion batteries, Adv. Sci. 9 (22) (2022) 2201207, https://doi.org/10.1002/advs.202201207.
[80] X. Li, X. Wang, L. Ma, W. Huang, Solvation structures in aqueous metal-ion batteries, Adv. Energy Mater. 12 (37) (2022) 2202068, https://doi.org/10.1002/aenm.202202068.
[81] P. Xiong, F. Zhang, X. Zhang, Y. Liu, Y. Wu, S. Wang, J. Safaei, B. Sun, R. Ma, Z. Liu, Atomic-scale regulation of anionic and cationic migration in alkali metal batteries, Nat. Commun. 12 (1) (2021) 4184, https://doi.org/10.1038/s41467-021-24399-9.
[82] R. Hou, S. Guo, H. Zhou, Atomic insights into advances and issues in low-temperature electrolytes, Adv. Energy Mater. 13 (14) (2023) 2300053, https://doi.org/10.1002/aenm.202300053.
[83] J.F. Ding, R. Xu, N. Yao, X. Chen, Y. Xiao, Y.X. Yao, C. Yan, J. Xie, J.Q. Huang, Non-solvating and low-dielectricity cosolvent for anion-derived solid electrolyte interphases in lithium metal batteries, Angew. Chem. Int. Ed. 60 (20) (2021) 11442–11447, https://doi.org/10.1002/anie.202101627.
[84] T. Li, X.Q. Zhang, N. Yao, Y.X. Yao, L.P. Hou, X. Chen, M.Y. Zhou, J.Q. Huang, Q. Zhang, Stable anion-derived solid electrolyte interphase in lithium metal batteries, Angew. Chem. Int. Ed. 60 (42) (2021) 22683–22687, https://doi.org/10.1002/ange.202107732.
[85] H. Chu, J. Jung, H. Noh, S. Yuk, J. Lee, J.H. Lee, J. Baek, Y. Roh, H. Kwon, D. Choi, Unraveling the dual functionality of high-donor-number anion in lean-electrolyte lithium-sulfur batteries, Adv. Energy Mater. 10 (21) (2020) 2000493, https://doi.org/10.1002/aenm.202000493.
[86] N. Piao, X. Gao, H. Yang, Z. Guo, G. Hu, H.-M. Cheng, F. Li, Challenges and development of lithium-ion batteries for low temperature environments, Etransportation 11 (2022) 100145, https://doi.org/10.1016/j.etran.2021.100145.
[87] Q. Li, D. Lu, J. Zheng, S. Jiao, L. Luo, C.-M. Wang, K. Xu, J.-G. Zhang, W. Xu, Li^+-desolvation dictating lithium-ion battery's low-temperature performances, ACS. Appl. Mater. Interfaces. 9 (49) (2017) 42761–42768, https://doi.org/10.1021/acsami.7b13887.
[88] N. Bensalah, Y. De Luna, Recent progress in layered manganese and vanadium oxide cathodes for Zn-ion batteries, Energy Technol. 9 (5) (2021) 2100011, https://doi.org/10.1002/ente.202100011.
[89] Y. Zou, X. Yang, L. Shen, Y. Su, Z. Chen, X. Gao, J. Zhou, J. Sun, Emerging strategies for steering orientational deposition toward high-performance Zn metal anodes, Energy Environ. Sci. 15 (12) (2022) 5017–5038, https://doi.org/10.1039/d2ee02416k.
[90] H. Jia, Z. Wang, B. Tawiah, Y. Wang, C.-Y. Chan, B. Fei, F. Pan, Recent advances in zinc anodes for high-performance aqueous Zn-ion batteries, Nano Energy 70 (2020) 104523, https://doi.org/10.1016/j.nanoen.2020.104523.
[91] Z. Zhang, Y. Li, R. Xu, W. Zhou, Y. Li, S.T. Oyakhire, Y. Wu, J. Xu, H. Wang, Z. Yu, Capturing the swelling of solid-electrolyte interphase in lithium metal batteries, Science (1979) 375 (6576) (2022) 66–70, https://doi.org/10.1126/science.abi8703.
[92] A. Smith, J.C. Burns, X. Zhao, D. Xiong, J. Dahn, A high precision coulometry study of the SEI growth in Li/graphite cells, J. Electrochem. Soc. 158 (5) (2011) A447, https://doi.org/10.1149/1.3557892.
[93] W. Deng, W. Dai, X. Zhou, Q. Han, W. Fang, N. Dong, B. He, Z. Liu, Competitive solvation-induced concurrent protection on the anode and cathode toward a 400 Wh kg^{-1} lithium metal battery, ACS. Energy Lett. 6 (1) (2020) 115–123, https://doi.org/10.1021/acsenergylett.0c02351.
[94] X.-Q. Zhang, X. Chen, L.-P. Hou, B.-Q. Li, X.-B. Cheng, J.-Q. Huang, Q. Zhang, Regulating anions in the solvation sheath of lithium ions for stable lithium metal batteries, ACS. Energy Lett. 4 (2) (2019) 411–416, https://doi.org/10.1021/acsenergylett.8b02376.
[95] Y.X. Yao, X. Chen, N. Yao, J.H. Gao, G. Xu, J.F. Ding, C.L. Song, W.L. Cai, C. Yan, Q. Zhang, Unlocking charge transfer limitations for extreme fast charging of Li-ion batteries, Angew. Chem. 135 (4) (2023) e202214828, https://doi.org/10.1002/ange.202214828.
[96] B. Nan, L. Chen, N.D. Rodrigo, O. Borodin, N. Piao, J. Xia, T. Pollard, S. Hou, J. Zhang, X. Ji, Enhancing Li^+ transport in NMC811|| graphite lithium-ion batteries at low temperatures by using low-polarity-solvent electrolytes, Angew. Chem. Int. Ed. 61 (35) (2022) e202205967, https://doi.org/10.1002/ange.202205967.
[97] K. Xu, A. von Cresce, U. Lee, Differentiating contributions to "ion transfer" barrier from interphasial resistance and Li^+ desolvation at electrolyte/graphite interface, Langmuir. 26 (13) (2010) 11538–11543, https://doi.org/10.1021/la1009994.
[98] Z. Wang, F. Qi, L. Yin, Y. Shi, C. Sun, B. An, H.M. Cheng, F. Li, An anion-tuned solid electrolyte interphase with fast ion transfer kinetics for stable lithium anodes, Adv. Energy Mater. 10 (14) (2020) 1903843, https://doi.org/10.1002/aenm.201903843.
[99] Y. Wang, X. Yang, Z. Zhang, X. Hu, Y. Meng, X. Wang, D. Zhou, H. Liu, B. Li, G. Wang, Electrolyte design for rechargeable anion shuttle batteries, eScience 2 (6) (2022) 573–590, https://doi.org/10.1016/j.esci.2022.10.003.
[100] Y. Dong, H. Hu, P. Liang, L. Xue, X. Chai, F. Liu, M. Yu, F. Cheng, Dissolution, solvation and diffusion in low-temperature zinc electrolyte design, Nat. Rev. Chem. 9 (2) (2025) 102–117, https://doi.org/10.1038/s41570-024-00670-7.
[101] C. Cui, D. Han, H. Lu, Z. Li, K. Zhang, B. Zhang, X. Guo, R. Sun, X. Ye, J. Gao, Breaking consecutive hydrogen-bond network toward high-rate hydrous organic zinc batteries, Adv. Energy Mater. 13 (31) (2023) 2301466, https://doi.org/10.1002/aenm.202301466.
[102] C. Cárdenas, N. Rabi, P.W. Ayers, C. Morell, P. Jaramillo, P. Fuentealba, Chemical reactivity descriptors for ambiphilic reagents: dual descriptor, local hypersoftness, and electrostatic potential, J. Phys. Chem. A 113 (30) (2009) 8660–8667, https://doi.org/10.1021/jp902792n.
[103] P. Liang, H. Hu, Y. Dong, Z. Wang, K. Liu, G. Ding, F. Cheng, Competitive coordination of ternary anions enabling fast Li-ion desolvation for low-temperature lithium metal batteries, Adv. Funct. Mater. 34 (16) (2024) 2309858, https://doi.org/10.1002/adfm.202309858.
[104] G. Yang, J. Huang, X. Wan, B. Liu, Y. Zhu, J. Wang, O. Fontaine, S. Luo, P. Hiralal, Y. Guo, An aqueous zinc-ion battery working at −50°C enabled by low-concentration perchlorate-based chaotropic salt electrolyte, EcoMat. 4 (2) (2022) e12165, https://doi.org/10.1002/eom2.12165.
[105] S. Chakrabarty, E.R. Williams, The effect of halide and iodate anions on the hydrogen-bonding network of water in aqueous nanodrops, Phys. Chem. Chem. Phys. 18 (36) (2016) 25483–25490, https://doi.org/10.1039/c6cp05033f.
[106] Y. Tang, J.H. Li, C.L. Xu, M. Liu, B. Xiao, P.F. Wang, Electrode/electrolyte interfacial engineering for aqueous Zn-ion batteries, Carbon Neutralization 2 (2) (2023) 186–212, https://doi.org/10.1002/cnl2.54.
[107] D. Wang, T. He, A. Wang, K. Guo, M. Avdeev, C. Ouyang, L. Chen, S. Shi, A thermodynamic cycle-based electrochemical windows database of 308 electrolyte solvents for rechargeable batteries, Adv. Funct. Mater. 33 (11) (2023) 2212342, https://doi.org/10.1002/adfm.202212342.
[108] K. Chen, X. Shen, L. Luo, H. Chen, R. Cao, X. Feng, W. Chen, Y. Fang, Y. Cao, Correlating the solvating power of solvents with the strength of ion-dipole interaction in electrolytes of lithium-ion batteries, Angew. Chem. 135 (47) (2023) e202312373, https://doi.org/10.1002/ange.202312373.
[109] X. Chen, Q. Zhang, Atomic insights into the fundamental interactions in lithium battery electrolytes, Acc. Chem. Res. 53 (9) (2020) 1992–2002, https://doi.org/10.1021/acs.accounts.0c00412.
[110] X. Chen, X.Q. Zhang, H.R. Li, Q.J.B. Zhang, Supercaps, Cation−solvent, cation−anion, and solvent−solvent interactions with electrolyte solvation in

lithium batteries, Batter. Supercaps. 2 (2) (2019) 128–131, https://doi.org/10.1002/batt.201900006.
[111] P. Lai, Y. Zhang, B. Huang, X. Deng, H. Hua, Q. Chen, S. Zhao, J. Dai, P. Zhang, J. Zhao, Revealing the evolution of solvation structure in low-temperature electrolytes for lithium batteries, Energy Storage Mater. 67 (2024) 103314, https://doi.org/10.1016/j.ensm.2024.103314.
[112] J. Holoubek, K. Yu, J. Wu, S. Wang, M. Li, H. Gao, Z. Hui, G. Hyun, Y. Yin, A. U. Mu, Toward a quantitative interfacial description of solvation for Li metal battery operation under extreme conditions, Proc. Natl. Acad. Sci. 120 (41) (2023) e2310714120, https://doi.org/10.1073/pnas.2310714120.
[113] C. Yang, X. Liu, Y. Lin, L. Yin, J. Lu, Y. You, Entropy-driven solvation toward low-temperature sodium-ion batteries with temperature-adaptive feature, Adv. Mater. 35 (28) (2023) 2301817, https://doi.org/10.1002/adma.202301817.
[114] Q. Lin, D. Kundu, M. Skyllas-Kazacos, J. Lu, D. Zhao, K. Amine, L. Dai, D. W. Wang, Perspective on Lewis Acid-Base Interactions in Emerging Batteries, Adv. Mater. 36 (42) (2024) 2406151, https://doi.org/10.1002/adma.202406151.
[115] G. Leverick, Y. Shao-Horn, Controlling electrolyte properties and redox reactions using solvation and implications in battery functions: a Mini-Review, Adv. Energy Mater. 13 (13) (2023) 2204094, https://doi.org/10.1002/aenm.202204094.
[116] R. Mancinelli, A. Botti, F. Bruni, M. Ricci, A. Soper, Perturbation of water structure due to monovalent ions in solution, Phys. Chem. Chem. Phys. 9 (23) (2007) 2959–2967, https://doi.org/10.1039/b701855j.
[117] T. Sun, X. Yuan, K. Wang, S. Zheng, J. Shi, Q. Zhang, W. Cai, J. Liang, Z. Tao, An ultralow-temperature aqueous zinc-ion battery, J. Mater. Chem. A 9 (11) (2021) 7042–7047, https://doi.org/10.1039/d0ta12409e.
[118] T. Sun, H. Du, S. Zheng, J. Shi, Z. Tao, High power and energy density aqueous proton battery operated at− 90°C, Adv. Funct. Mater. 31 (16) (2021) 2010127, https://doi.org/10.1002/adfm.202010127.
[119] K. Nieszporek, J. Nieszporek, Multi-centred hydrogen bonds between water and perchlorate anion, Phys. Chem. Liquids 55 (4) (2017) 473–481, https://doi.org/10.1080/00319104.2016.1227811.
[120] K. Zhu, Z. Li, Z. Sun, P. Liu, T. Jin, X. Chen, H. Li, W. Lu, L. Jiao, Inorganic electrolyte for low-temperature aqueous sodium ion batteries, Small. 18 (14) (2022) 2107662, https://doi.org/10.1002/smll.202107662.
[121] L. Jiang, Y.-C. Lu, Building a long-lifespan aqueous k-ion battery operating at −35 °C, ACS. Energy Lett. 9 (3) (2024) 985–991, https://doi.org/10.1021/acsenergylett.4c00098.
[122] L. Jiang, Y. Lu, C. Zhao, L. Liu, J. Zhang, Q. Zhang, X. Shen, J. Zhao, X. Yu, H. Li, Building aqueous K-ion batteries for energy storage, Nat. Energy 4 (6) (2019) 495–503, https://doi.org/10.1038/s41560-019-0388-0.
[123] H. Wang, H. Zhang, Y. Cheng, K. Feng, X. Li, H. Zhang, All-NASICON LVP-LTP aqueous lithium ion battery with excellent stability and low-temperature performance, Electrochim. Acta 278 (2018) 279–289, https://doi.org/10.1016/j.electacta.2018.05.047.
[124] D. Xiao, L. Zhang, Z. Li, H. Dou, X. Zhang, Design strategies and research progress for Water-in-Salt electrolytes, Energy Storage Mater. 44 (2022) 10–28, https://doi.org/10.1016/j.ensm.2021.09.035.
[125] C. You, W. Fan, X. Xiong, H. Yang, L. Fu, T. Wang, F. Wang, Z. Zhu, J. He, Y. Wu, Design strategies for anti-freeze electrolytes in aqueous energy storage devices at low temperatures, Adv. Funct. Mater. 34 (40) (2024) 2403616, https://doi.org/10.1002/adfm.202403616.
[126] Y. He, Z. Chen, J. Feng, J. Wang, L. Zhang, H. Gu, L. Sheng, P. Yao, F.R. Wang, Z. Hao, Highly reversible aqueous zinc-ion batteries via multifunctional hydrogen-bond-rich dulcitol at lower temperature, Small. 21 (11) (2025) 2411755, https://doi.org/10.1002/smll.202411755.
[127] B. Hu, T. Chen, Y. Wang, X. Qian, Q. Zhang, J. Fu, Reconfiguring the electrolyte network structure with bio-inspired cryoprotective additive for low-temperature aqueous zinc batteries, Adv. Energy Mater. 14 (31) (2024) 2401470, https://doi.org/10.1002/aenm.202401470.
[128] C. Tang, M. Li, J. Du, Y. Wang, Y. Zhang, G. Wang, X. Shi, Y. Li, J. Liu, C. Lian, L. Li, Supramolecular-induced 2.40 V 130 °C working-temperature-range supercapacitor aqueous electrolyte of lithium bis(trifluoromethanesulfonyl) imide in dimethyl sulfoxide-water, J. Colloid. Interface Sci. 608 (2022) 1162–1172, https://doi.org/10.1016/j.jcis.2021.10.090.
[129] Y. Liu, L. Miao, H. Shen, Z. Wang, K. Yao, Y. Hu, J. Sun, S. Hou, J. Zhao, K. Yang, Maximizing functional diversity of electrolyte additives through modular molecular engineering to stabilize zinc metal anodes, Adv. Funct. Mater. 35 (30) (2025) 2501968, https://doi.org/10.1002/adfm.202501968.
[130] J. Wei, P. Zhang, T. Shen, Y. Liu, T. Dai, Z. Tie, Z. Jin, Supramolecule-based excluded-volume electrolytes and conjugated sulfonamide cathodes for high-voltage and long-cycling aqueous zinc-ion batteries, ACS. Energy Lett. 8 (1) (2022) 762–771, https://doi.org/10.1021/acsenergylett.2c02646.
[131] D. Feng, F. Cao, L. Hou, T. Li, Y. Jiao, P. Wu, Immunizing aqueous Zn batteries against dendrite formation and side reactions at various temperatures via electrolyte additives, Small. 17 (42) (2021) 2103195, https://doi.org/10.1002/smll.202103195.
[132] Q. Nian, J. Wang, S. Liu, T. Sun, S. Zheng, Y. Zhang, Z. Tao, J. Chen, Aqueous batteries operated at −50 °C, Angew. Chem. Int. Ed. 58 (47) (2019) 16994–16999, https://doi.org/10.1002/anie.201908913.
[133] Q. Nian, T. Sun, Y. Li, S. Jin, S. Liu, X. Luo, Z. Wang, B.Q. Xiong, Z. Cui, D. Ruan, H. Ji, Z. Tao, X. Ren, Regulating frozen electrolyte structure with colloidal dispersion for low temperature aqueous batteries, Angew. Chem. Int. Ed. 62 (9) (2023) e202217671, https://doi.org/10.1002/anie.202217671.
[134] W. Yang, X. Du, J. Zhao, Z. Chen, J. Li, J. Xie, Y. Zhang, Z. Cui, Q. Kong, Z. Zhao, Hydrated eutectic electrolytes with ligand-oriented solvation shells for long-cycling zinc-organic batteries, Joule 4 (7) (2020) 1557–1574, https://doi.org/10.1016/j.joule.2020.05.018.
[135] J. Wang, Q. Zhu, F. Li, J. Chen, H. Yuan, Y. Li, P. Hu, M.S. Kurbanov, H. Wang, Low-temperature and high-rate Zn metal batteries enabled by mitigating Zn^{2+} concentration polarization, Chem. Eng. J. 433 (2022) 134589, https://doi.org/10.1016/j.cej.2022.134589.
[136] X. Shi, J. Wang, F. Yang, X. Liu, Y. Yu, X. Lu, Metallic zinc anode working at 50 and 50 mAh cm^{-2} with high depth of discharge via electrical double layer reconstruction, Adv. Funct. Mater. 33 (7) (2023) 2211917, https://doi.org/10.1002/adfm.202211917.
[137] Q. Dong, H. Ao, Z. Qin, Z. Xu, J. Ye, Y. Qian, Z. Hou, Synergistic chaotropic effect and cathode interface thermal release effect enabling ultralow temperature aqueous zinc battery, Small. 18 (44) (2022) 2203347, https://doi.org/10.1002/smll.202203347.
[138] A. Duan, S. Luo, W. Sun, Insight into the development of electrolytes for aqueous zinc metal batteries from alkaline to neutral, Chin. Chem. Lett. 35 (2) (2024) 108337, https://doi.org/10.1016/j.cclet.2023.108337.
[139] B. Wu, Y. Mu, Z. Li, M. Li, L. Zeng, T. Zhao, Realizing high-voltage aqueous zinc-ion batteries with expanded electrolyte electrochemical stability window, Chin. Chem. Lett. 34 (2) (2023) 107629, https://doi.org/10.1016/j.cclet.2022.06.052.
[140] T.T. Liu, C.J. Lei, H.J. Wang, J.Y. Li, P.J. Jiang, X. He, X. Liang, Aqueous electrolyte with weak hydrogen bonds for four-electron zinc-iodine battery operates in a wide temperature range, Adv. Mater. 36 (32) (2024) 2405473, https://doi.org/10.1002/adma.202405473.
[141] K. Zhu, Z. Sun, Z. Li, P. Liu, X. Chen, L. Jiao, Aqueous sodium ion hybrid batteries with ultra-long cycle life at-50°C, Energy Storage Mater. 53 (2022) 523–531, https://doi.org/10.1016/j.ensm.2022.09.019.
[142] R. Qin, Y. Wang, M. Zhang, Y. Wang, S. Ding, A. Song, H. Yi, L. Yang, Y. Song, Y. Cui, Tuning Zn^{2+} coordination environment to suppress dendrite formation for high-performance Zn-ion batteries, Nano Energy 80 (2021) 105478, https://doi.org/10.1016/j.nanoen.2020.105478.
[143] Y. Wu, Z. Zhu, D. Shen, L. Chen, T. Song, T. Kang, Z. Tong, Y. Tang, H. Wang, C. S. Lee, Electrolyte engineering enables stable Zn-ion deposition for long-cycling life aqueous Zn-ion batteries, Energy Storage Mater. 45 (2022) 1084–1091, https://doi.org/10.1016/j.ensm.2021.11.003.
[144] J. Chen, J. Vatamanu, L. Xing, O. Borodin, H. Chen, X. Guan, X. Liu, K. Xu, W. Li, Improving electrochemical stability and low-temperature performance with water/acetonitrile hybrid electrolytes, Adv. Energy Mater. 10 (3) (2020) 1902654, https://doi.org/10.1002/aenm.201902654.
[145] Q. Dou, S. Lei, D.-W. Wang, Q. Zhang, D. Xiao, H. Guo, A. Wang, H. Yang, Y. Li, S. Shi, Safe and high-rate supercapacitors based on an "acetonitrile/water in salt" hybrid electrolyte, Energy Environ. Sci. 11 (11) (2018) 3212–3219, https://doi.org/10.1039/c8ee01040d.
[146] M. Nagaraju, G. Narahari Sastry, Comparative study on formamide–water complex, Int. J. Quantum. Chem. 110 (10) (2010) 1994–2003, https://doi.org/10.1002/qua.22368.
[147] H. Liu, C. Zhao, X. Wu, C. Hu, F. Geng, M. Shen, B. Hu, B. Hu, C. Li, Inconsistency between superstructure stability and long-term cyclability of oxygen redox in Na layered oxides, Energy Environ. Sci. 17 (2) (2024) 668–679, https://doi.org/10.1039/d3ee02915h.
[148] B.B. Hansen, S. Spittle, B. Chen, D. Poe, Y. Zhang, J.M. Klein, A. Horton, L. Adhikari, T. Zelovich, B.W. Doherty, Deep eutectic solvents: a review of fundamentals and applications, Chem. Rev. 121 (3) (2020) 1232–1285, https://doi.org/10.1021/acs.chemrev.0c00385.
[149] M.A. Martins, S.P. Pinho, J.A. Coutinho, Insights into the nature of eutectic and deep eutectic mixtures, J. Solution. Chem. 48 (2019) 962–982, https://doi.org/10.1007/s10953-018-0793-1.
[150] W. Kao-ian, R. Pornprasertsuk, P. Thamyongkit, T. Maiyalagan, S. Kheawhom, Rechargeable zinc-ion battery based on choline chloride-urea deep eutectic solvent, J. Electrochem. Soc. 166 (6) (2019) A1063–A1069, https://doi.org/10.1149/2.0641906jes.
[151] W. Lv, Y. Tan, C. Guo, X. He, L. Zeng, J. Zhu, L. Yang, Z. Chen, X. Yin, J. Xu, Triple regulation of water molecules behavior to realize high stability and broad temperature tolerance in aqueous zinc metal batteries via a novel cost-effective eutectic electrolyte, Adv. Energy Mater. 15 (15) (2025) 2403689, https://doi.org/10.1002/aenm.202403689.
[152] N. Chang, T. Li, R. Li, S. Wang, Y. Yin, H. Zhang, X. Li, An aqueous hybrid electrolyte for low-temperature zinc-based energy storage devices, Energy Environ. Sci. 13 (10) (2020) 3527–3535, https://doi.org/10.1039/d0ee01538e.
[153] X. Zhang, R. Wang, Z. Liu, Q. Ma, H. Li, Y. Liu, J. Hao, S. Zhang, J. Mao, C. Zhang, Regulated hydrated eutectic electrolyte enhancing interfacial chemical stability for highly reversible aqueous aluminum-ion battery with a wide temperature range of-20 to 60 °C, Adv. Energy Mater. 14 (22) (2024) 2400314, https://doi.org/10.1002/aenm.202400314.
[154] Z. Liu, X. Luo, L. Qin, G. Fang, S. Liang, Progress and prospect of low-temperature zinc metal batteries, Adv. Powder Mater. 1 (2) (2022) 100011, https://doi.org/10.1016/j.apmate.2021.10.002.
[155] T. Xiong, Y. Guo, X. Wang, Design and structure of electrolytes for all-weather aqueous zinc batteries, Adv. Funct. Mater. 35 (16) (2024) 2421240, https://doi.org/10.1002/adfm.202421240.
[156] T. Sun, S. Zheng, H. Du, Z. Tao, Synergistic effect of cation and anion for low-temperature aqueous zinc-ion battery, Nanomicro Lett. 13 (2021) 1–10, https://doi.org/10.1007/s40820-021-00733-0.
[157] G. Horwitz, E. Härk, P.Y. Steinberg, L.P. Cavalcanti, S. Risse, H.R. Corti, The nanostructure of water-in-salt electrolytes revisited: effect of the anion size, ACS. Nano 15 (7) (2021) 11564–11572, https://doi.org/10.1021/acsnano.1c01737.

[158] J. Lim, K. Park, H. Lee, J. Kim, K. Kwak, M. Cho, Nanometric water channels in water-in-salt lithium ion battery electrolyte, J. Am. Chem. Soc. 140 (46) (2018) 15661–15667, https://doi.org/10.1021/jacs.8b07696.
[159] D. Reber, R. Grissa, M. Becker, R.S. Kühnel, C. Battaglia, Anion selection criteria for water-in-salt electrolytes, Adv. Energy Mater. 11 (5) (2021) 2002913, https://doi.org/10.1002/aenm.202002913.
[160] D.M. Seo, T. Afroz, J.L. Allen, P.D. Boyle, P.C. Trulove, H.C. De Long, W. A. Henderson, Structural interactions within lithium salt solvates: cyclic carbonates and esters, J. Phys. Chem. C 118 (45) (2014) 25884–25889, https://doi.org/10.1021/jp5079168.
[161] N. Chapman, O. Borodin, T. Yoon, C.C. Nguyen, B.L. Lucht, Spectroscopic and density functional theory characterization of common lithium salt solvates in carbonate electrolytes for lithium batteries, J. Phys. Chem. C 121 (4) (2017) 2135–2148, https://doi.org/10.1021/acs.jpcc.6b12234.
[162] X. Lu, J.M. Vicent-Luna, S. Calero, R.M. Madero-Castro, M.C. Gutiérrez, M. L. Ferrer, F. del Monte, EMIMBF4 in ternary liquid mixtures of water, dimethyl sulfoxide and acetonitrile as "tri-solvent-in-salt" electrolytes for high-performance supercapacitors operating at-70 ℃, Energy Storage Mater. 40 (2021) 368–385, https://doi.org/10.1016/j.ensm.2021.05.026.
[163] Y. Yamada, Y. Koyama, T. Abe, Z. Ogumi, Correlation between charge− discharge behavior of graphite and solvation structure of the lithium ion in propylene carbonate-containing electrolytes, J. Phys. Chem. C 113 (20) (2009) 8948–8953, https://doi.org/10.1021/jp9022458.
[164] S.-K. Jeong, M. Inaba, Y. Iriyama, T. Abe, Z. Ogumi, Electrochemical intercalation of lithium ion within graphite from propylene carbonate solutions, Electrochem. Solid-State Lett. 6 (1) (2002) A13, https://doi.org/10.1149/1.1526781.
[165] Z. Peng, X. Cao, P. Gao, H. Jia, X. Ren, S. Roy, Z. Li, Y. Zhu, W. Xie, D. Liu, High-power lithium metal batteries enabled by high-concentration acetonitrile-based electrolytes with vinylene carbonate additive, Adv. Funct. Mater. 30 (24) (2020) 2001285, https://doi.org/10.1002/adfm.202001285.
[166] X. Ren, X. Zhang, Z. Shadike, L. Zou, H. Jia, X. Cao, M.H. Engelhard, B. E. Matthews, C. Wang, B.W. Arey, Designing advanced in situ electrode/electrolyte interphases for wide temperature operation of 4.5 V Li|| $LiCoO_2$ batteries, Adv. Mater. 32 (49) (2020) 2004898, https://doi.org/10.1002/adma.202004898.
[167] M. Yang, J. Zhu, S. Bi, R. Wang, Z. Niu, A binary hydrate-melt electrolyte with acetate-oriented cross-linking solvation shells for stable zinc anodes, Adv. Mater. 34 (18) (2022) 2201744, https://doi.org/10.1002/adma.202201744.
[168] Q. Zhang, Y. Ma, Y. Lu, X. Zhou, L. Lin, L. Li, Z. Yan, Q. Zhao, K. Zhang, J. Chen, Designing anion-type water-free Zn^{2+} solvation structure for robust Zn metal anode, Angew. Chem. Int. Ed. 60 (43) (2021) 23357–23364, https://doi.org/10.1002/ange.202109682.
[169] S.R. Alfarano, S. Pezzotti, C.J. Stein, Z. Lin, F. Sebastiani, S. Funke, C. Hoberg, I. Kolling, C.Y. Ma, K. Mauelshagen, Stripping away ion hydration shells in electrical double-layer formation: water networks matter, Proc. Natl. Acad. Sci. 118 (47) (2021) e2108568118, https://doi.org/10.1073/pnas.2108568118.
[170] J. Fan, Q. Li, Y. Chen, J. Cui, D. Shan, X. Lv, H. Tu, Y. Zhang, Y. Wu, Y. Chen, Regulating the solvation structures through high-entropy strategy for wide-temperature zinc-ion batteries, J. Mater. Chem. A 13 (21) (2025) 16070–16080, https://doi.org/10.1039/d5ta00937e.
[171] R. Wang, Q. Ma, L. Zhang, Z. Liu, J. Wan, J. Mao, H. Li, S. Zhang, J. Hao, L. Zhang, C. Zhang, An aqueous electrolyte regulator for highly stable zinc anode under-35 to 65 °C, Adv. Energy Mater. 13 (40) (2023) 2302543, https://doi.org/10.1002/aenm.202302543.
[172] Y. Dong, N. Zhang, Z. Wang, J. Li, Y. Ni, H. Hu, F. Cheng, Cell-nucleus structured electrolyte for low-temperature aqueous zinc batteries, J. Energy Chem. 83 (2023) 324–332, https://doi.org/10.1016/j.jechem.2023.04.017.
[173] Y. Liu, K. Feng, J. Han, F. Wang, Y. Xing, F. Tao, H. Li, B. Xu, J. Ji, H. Li, Regulation of Zn^{2+} solvation shell by a novel N-methylacetamide based eutectic electrolyte toward high-performance zinc-ion batteries, J. Mater. Sci. Technol. 211 (2025) 53–61, https://doi.org/10.1016/j.jmst.2024.05.030.
[174] D. Wang, Q. Li, Y. Zhao, H. Hong, H. Li, Z. Huang, G. Liang, Q. Yang, C. Zhi, Insight on organic molecules in aqueous Zn-ion batteries with an emphasis on the Zn anode regulation, Adv. Energy Mater. 12 (9) (2022) 2102707, https://doi.org/10.1002/aenm.202102707.
[175] S. Bai, Z. Huang, G. Liang, R. Yang, D. Liu, W. Wen, X. Jin, C. Zhi, X. Wang, Electrolyte additives for stable Zn anodes, Adv. Sci. 11 (4) (2024) 2304549, https://doi.org/10.1002/advs.202304549.
[176] K. Zhao, G. Fan, J. Liu, F. Liu, J. Li, X. Zhou, Y. Ni, M. Yu, Y.-M. Zhang, H. Su, Boosting the kinetics and stability of Zn anodes in aqueous electrolytes with supramolecular cyclodextrin additives, J. Am. Chem. Soc. 144 (25) (2022) 11129–11137, https://doi.org/10.1021/jacs.2c00551.
[177] W. Zhong, Z. Shen, J. Mao, S. Zhang, H. Cheng, Y. Kim, Y. Lu, Mitigating cathodic dissolution through interfacial water masking to enhance the longevity of aqueous zinc–ion batteries, Energy Environ. Sci. 17 (5) (2024) 2059–2068, https://doi.org/10.1039/d3ee04208a.
[178] F. Yang, J.A. Yuwono, J. Hao, J. Long, L. Yuan, Y. Wang, S. Liu, Y. Fan, S. Zhao, K. Davey, Understanding H_2 evolution electrochemistry to minimize solvated water impact on Zinc-anode performance, Adv. Mater. 34 (45) (2022) 2206754, https://doi.org/10.1002/adma.202206754.
[179] Y. Qiu, Y. Lin, D. Shi, H. Zhang, J. Luo, J. Chen, Z. Liu, Y. Yu, D. Lin, W. Zhang, Möbius solvation structure for zinc-ion batteries, Adv. Mater. 37 (13) (2025) 2415373, https://doi.org/10.1002/adma.202415373.
[180] L. Yu, J. Huang, S. Wang, L. Qi, S. Wang, C. Chen, Ionic liquid "water pocket" for stable and environment-adaptable aqueous zinc metal batteries, Adv. Mater. 35 (21) (2023) 2210789, https://doi.org/10.1002/adma.202210789.
[181] F. Ming, Y. Zhu, G. Huang, A.-H. Emwas, H. Liang, Y. Cui, H.N. Alshareef, Co-solvent electrolyte engineering for stable anode-free zinc metal batteries, J. Am. Chem. Soc. 144 (16) (2022) 7160–7170, https://doi.org/10.1021/jacs.1c12764.
[182] Y. Deng, H. Wang, M. Fan, B. Zhan, L.-J. Zuo, C. Chen, L. Yan, Nanomicellar electrolyte to control release ions and reconstruct hydrogen bonding network for ultrastable high-energy-density Zn–Mn battery, J. Am. Chem. Soc. 145 (36) (2023) 20109–20120, https://doi.org/10.1021/jacs.3c07764.